THE UNIVERSITY OF TURKISH AERONAUTICAL ASSOCIATION
INSTITUTE OF SCIENCE AND TECHNOLOGY

NUMERICAL METHODS FOR PITCH MORPHING BLADE DESIGN FOR VERTICAL-TAKE-OFF-LANDING UNMANNED AERIAL SYSTEMS

MASTER THESIS

Mürüvvet Sinem SİCİM
1403730045

INSTITUTE OF SCIENCE AND TECHNOLOGY
MECHANICAL AND AERONAUTICAL ENGINEERING PROGRAM

THE UNIVERSITY OF TURKISH AERONAUTICAL ASSOCIATION
INSTITUTE OF SCIENCE AND TECHNOLOGY

NUMERICAL METHODS FOR PITCH MORPHING BLADE DESIGN FOR VERTICAL-TAKE-OFF-LANDING UNMANNED AERIAL SYSTEMS

MASTER THESIS

Mürüvvet Sinem SİCİM
1403730045

INSTITUTE OF SCIENCE AND TECHNOLOGY
MECHANICAL AND AERONAUTICAL ENGINEERING PROGRAM

Advisor: Assist. Prof. Dr. Durmuş Sinan KÖRPE

Mürüvvet Sinem SİCİM having student number 1403730045 and enrolled in the Master Program at the Institute of Science and Technology at the University of Turkish Aeronautical Association, after meeting all of the required conditions contained in the related regulations, has succeussfully accomplished, in front of the jury, the presentation of the thesis prepared with the title of: "NUMERICAL METHODS FOR PITCH MORPHING BLADE DESIGN FOR VERTICAL-TAKE-OFF-LANDING UNMANNED AERIAL SYSTEMS."

Superviser : Assist. Prof. Dr.Durmuş Sinan KÖRPE .....
University of Turkish Aeronautical Association

Jury Member : Assoc. Prof. Dr. Murat DEMİRAL .....
Çankaya University

Assist. Prof. Dr. Mohamed Salem ELMNEFİ .....
University of Turkish Aeronautical Association

Assist. Prof. Dr.Durmuş Sinan KÖRPE .....
University of Turkish Aeronautical Association

Thesis defence date: 11.08.2017

UNIVERSITY OF TURKISH AERONAUTICAL ASSOCIATION
INSTITUTE OF SCIENCE AND TECHNOLOGY

I hereby declare that all the information in this document has been obtained and presented in accordance with academic rules and ethical conduct. I also declare that, as required by these rules and conduct, I have fully cited and referenced all material and results that are not original to this work.

11/08/2017

Mürüvvet Sinem SİCİM

ACKNOWLEDGEMENTS

The author would like to thank Yrd. Doç. Dr. Sinan DURMUS for his guidance, support, encouragement and advice in support of the study. Thanks to Levent UNLUSOY who often have insights into problems from a different point of view and patience throughout the study. My gratitude goes out to him.
Dr. Sait Nurdogan YURT who study as a chef engineer in Turkish Airlines and has a background in İstanbul Technical University always support me psychologically to finish this thesis. I appreciate to Dinçer DEMİRCİ helps me during analysis process and encourage me until end of the thesis. Thank you to my parents as well as my mother Afife who is a retired teacher for all of their support and encouragement.

Mürüvvet Sinem SİCİM

TABLE OF CONTENTS

LIST OF TABLES

LIST OF FIGURES

NOMENCLATURE

A = amplitude of vibration

dij = piezoelectric constant relating voltage and stress

E = parameter at constant electrical field (short circuit)

V = volume

$\boldsymbol{\alpha_{ij}}$ = Thermal expansion coefficient

$\Delta\mathbf{T}$ = Change in temperature

Δ_{ES} = Elektrode spacing

c = Chord length

t = Thickness

t/c = Thickness to chord ratio

LIST OF ABBREVIATIONS

ADP **:**Ammoniumdihydrogen-Phosphate

AFC **:**Active Fiber Composite

DKT **:**Dipotoassium tartrate

EDT **:**Ethylene Diamine Tartrate

FSI **:**Fluid-Structure Interaction

GFPR **:**Glass Fiber Reinforced Polymer

HHC **:**Higher Harmonic Control

IBC **:**Individual Blade Control

MFC **:**Macro Fiber Composite

RAMS **:**Real-Time Aerial Monitoring System

ABSTRACT

NUMERICAL METHODS FOR PITCH MORPHING BLADE DESIGN FOR VERTICAL-TAKE-OFF-LANDING UNMANNED AERIAL SYSTEMS

Sicim, Mürüvvet Sinem

M.Sc., Department of Mechanical and Aeronautical Engineering

Advisor: Assis. Prof. Dr. Durmuş Sinan KÖRPE

Co-Advisor: Dr. Levent Ünlüsoy

July 2017, 74 pages

In this study, effects of morphing technologies on vibration reduction at vertical take-off landing unmanned aerial systems are observed. Helicopters are selected to be the main scope of investigation as a vertical take-off unmanned system. The effects of unsteady aerodynamics that amplifies the modes of vibration are believed to be reduced by the implementation of a twist morphing technology on the helicopter rotor blades. To obtain the twist technology, active piezoelectric fibers which are commonly called smart materials is embedded at ±45 deg orientation on the rotor blade. By applying a required amount of electrical voltage difference, they produce strain-induced twisting motions of the blade.

The effects of morphing on vibration reduction of the rotor blade were studied rather than the detailed design of the morphing blades. Therefore, blades are adopted from and then modelled a known unmanned helicopter's data such as Shark-120. The structural model of the wing was developed by using ANSYS/Workbench package program and all the analyses were conducted by using ANSYS/Workbench package program. The study shows that using piezoelectric actuator in active twist rotor method to reduce vibration of helicopter blade is highly efficient. Also, different piezoelectric arrangements and optimum voltages are determined. According to study, results conclude that torsion mode is used to determine the optimum placement of MFC

actuators. Also, the length of the MFC actuator and the voltage used in actuators affect rate of reduction in vibration.

Keywords: Unmanned Aerial Systems, Finite Element Analysis, Mission-Adaptive Helicopter Blade, Piezoelectric, Smart Material

ÖZET

DİKEY-İNİŞ-KALKIŞ-YAPAN İNSANSIZ HAVA SİSTEMLERİNDE HATVE DEĞİŞTİREBİLEN PALE TASARIMI İÇİN NÜMERİK ÇALIŞMA

Sicim, Mürüvvet Sinem
Yüksek Lisans, Makine ve Uçak Mühendisliği
Danışman: Yrd. Doç. Dr.Durmuş Sinan KÖRPE
Eş Danışman: Dr. Levent Ünlüsoy
Ağustos-2017, 74 pages

Bu çalışmada, dikey iniş kalkış yapan insansız hava araçlarında şekil değiştirebilme teknolojilerinin titreşim azaltma üzerindeki etkisi gözlemlenmiştir. Helikopterler dikey iniş kalkış yapabilen insansız hava sistemleri olarak ana araştırma alanı seçilmiştir. Büküm değiştirme teknolojisinin helikopter palleri üzerinde uygulanmasının titreşimi arttıran kararsız aerodinamiğin etkilerini azaltacağına inanılmaktadır. Bu teknolojiyi elde etmek için, akıllı malzeme olarak adlandırılan piezoelektrik fiberler $\pm 45^0$ oryantasyonunda pervane paline monte edilmektedir.

Bu tezde, şekil değiştirebilen palin detaylı tasarımından ziyede, şekil değiştirebilmne kabiliyetinin titreşim azaltma üzerindeki etkisi üzerine çalışılmıştır. Bu nedenle, paller insansız helicopter olarak bilinen Shark-120 nin dataları kabul edilerek tasarlanmıştır. Dikey kalkış iniş sistemi için kalkış konfigürasyonu temel parametredir. Kanadın yapısal modeli ANSYS/Workbench paket programı kullanılarak oluşturulmuş ve bütün analizler ANSYS/Workbench paket programı kullanılarak yapılmıştır.

Çalışma sonucunda akıllı malzemelerin aktif büküm değiştirme metodu kullanımıyla helicopter palleri üzerinde titreşim azaltımında oldukça etkili olduğu gözlemlenmiştir. Ayrıca, MFC eyleyici uzunluğu ve kullanılan voltajın titreşim azaltımı oranına etkisi incelenmiştir.

Anahtar Kelimeler: İnsansız Hava Araçları, Sonlu Elemanlar Analizi, Hatve Değiştirebilen Pale, Piezoelektrik, Akıllı Malzemeler

To my family

CHAPTER 1

INTRODUCTION

1.1 Background

Helicopter has the ability and necessary manoeuvrability is six-degrees-of-freedom within their missions and flight envelopes. Due to the several flight conditions during take-off, landing, hovering etc. which are characterizing a helicopter mission, it is nearly unattainable to answer the several design requirements with application of fixed rotor structure. When thoroughly investigated, through the forward flight of a helicopter, the rotor creates a very unique aerodynamic that requires a conventional swash-plate control. At this point, to avoid the complexity of swash-plate control, the blade can be twisted individually to various positions in flight to reach the design requirements and to optimize the pitch angle of blade to establish various flight conditions. Also, the angle of attack along the span can be changed individually according to flight conditions. For optimum performance, each blades are contained within helicopter rotor structure assembly should have the proper angle of attack. For a conventional blade, the twist distribution is passive regardless of the flight conditions so it can only sustain a selected flight condition.

During their operation, helicopter's overall performance decreases due to dynamic loading, excessive noise levels, aeromechanical instabilities etc. Vibration problem is one of the most serious issue due to causing discomfort for passenger/pilot and fatigue of the mechanical components. Active twist rotor blade approach is also used to vibration reduction. (Schulz, 2012)

As indicated in Figure 1, the main rotor experiences highly unsteady aerodynamic loads. According to figure, helicopter rotor region can be separated two

parts. They are categorized as advancing side and retreating side. In forward flight, both sides have different aerodynamic behaviour. The blade-vortex interactions cause unsteady aerodynamic loads on the advancing side and their effects are more powerful low forward flight speeds which is about $\mu = 0.15$. At the blade tip which is located on the advancing part of the rotor supercritical flow can be seen at higher advance ratios. However, on the retreating side, dynamic stall phenomena occur due to flow separation. At the root section which is located on the retreating side, flow over the airfoil is directed towards the leading edge from the trailing edge because opposing flow is observed in that region where forward flight speed is bigger than rotational speed. (Grimble & Johnson, 2016) Therefore, unsteady aerodynamics and structural deformations cause large oscillatory loads and vibration.

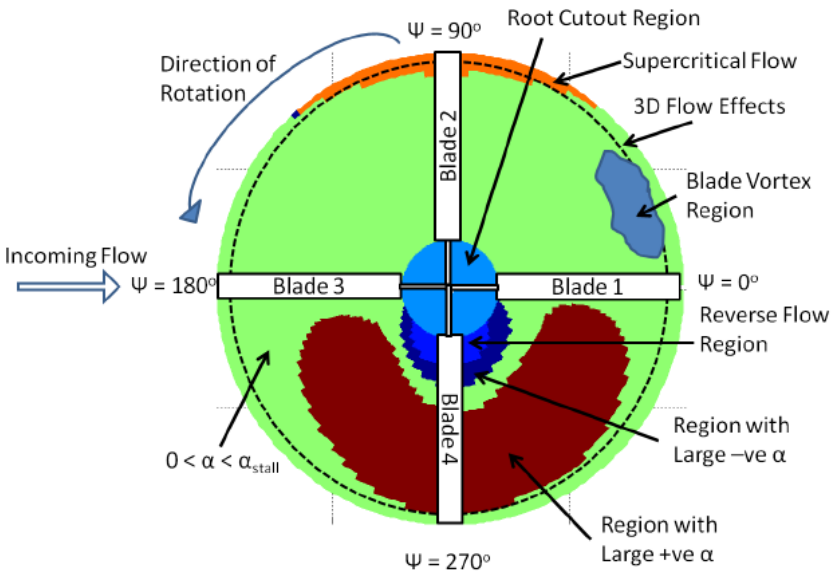

Figure 1: Unsteady Aerodynamics on the Main Rotor Disk (Kumar, 2013)

Figure 2 shows cabin vibration BO 105 helicopter with forward flight speed. At low speed, the blade-vortex interaction causes large vibration which is increased by the maneuvers retains the wake near the plane of the disk.

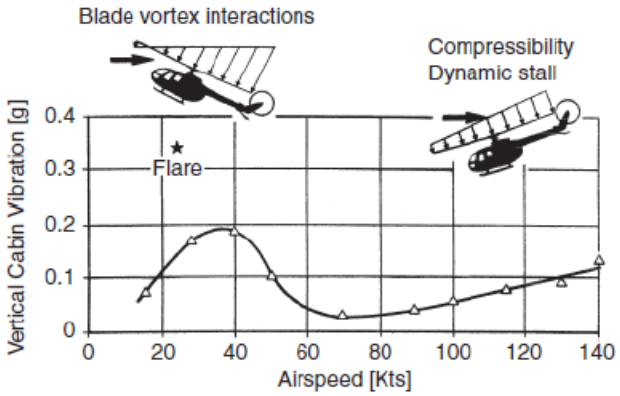

Figure 2: Vertical Cabin Vibration in BO 105 as a function of Airspeed (Kumar, 2013)

Also, dissymmetry of lift as shown in Figure 3 and Figure 4 is other means of the vibration of the main rotor. Dissymmetry of lift is the lift unbalance across the two sides of the rotor disk because dissimilar wind flow velocity contribution between each part. (Broderick , 2013) Wind velocity is summed up the rotational velocity on the advancing blade and diminished on other side of blade. Therefore, advancing side of blade can produce more lift than retreating side due to relative wind speed.

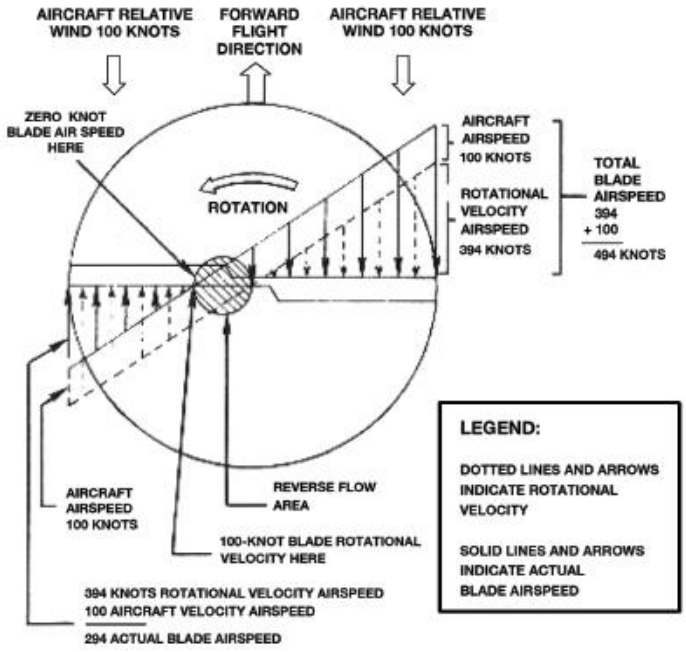

Figure 3: Dissymmetry of Lift 1 (Broderick , 2013)

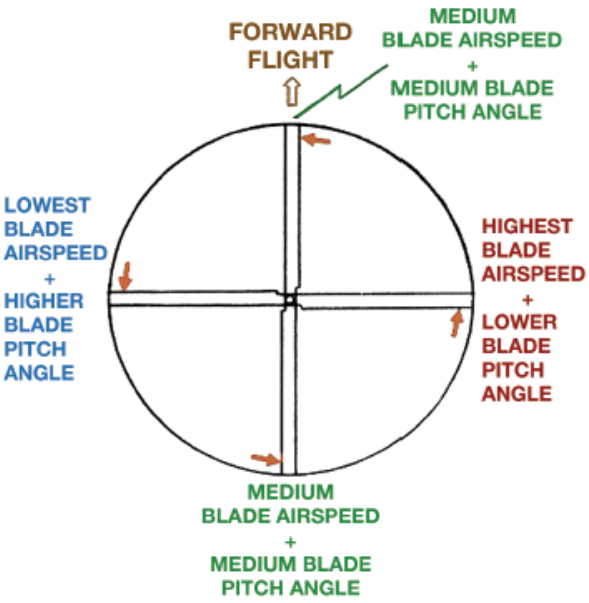

Figure 4: Dissymmetry of Lift 2 (Broderick , 2013)

1.2 Helicopter vibration control

Vibration reduction has been hot topic from the beginning of the design of the rotorcrafts. In literature, there are three approaches, named as; decreasing the source of vibration to eliminate the vibration, minimizing response of the structure to the vibration, insulating cabin from the source of vibration. Vibration reduction can be analysed in two different techniques: passive and active. The summary of the vibration reduction techniques in literature is shown in Figure 5.

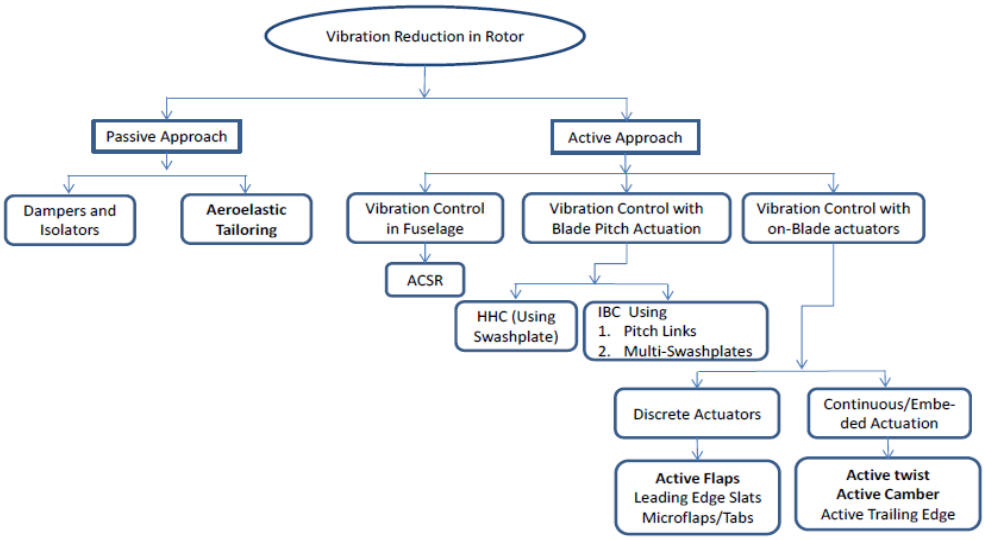

Figure 5: Methods used for Vibration Reduction in Rotor Blades. (Kumar, 2013)

The use of active controls to reduce vibrations in helicopters has been studied both analytically and experimentally for many years. Active techniques are most effective solution for reduction of vibration since they are directly affecting the source of vibratory loads. Active methods can be categorized by four methods. These methods are called as; higher harmonic control (HHC), İndividual Blade Control (IBC), active trailing-edge flap and active-twist rotor. In addition, HHC and IBC are under the section of blade pitch actuation.

Using actuator on the swash plate or pitch links to induce rigid body actuation influence aeroelastic behaviour of blade. Higher harmonic control (HHC, see Figure 6) reduces the vibration by application of active control of the swash plate which can change the pitch at the root.

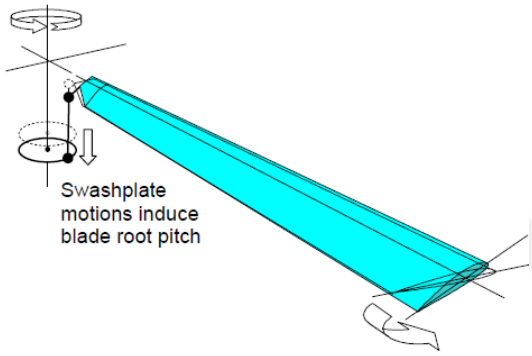

Figure 6: Higher Harmonic Control. (Wilbur & Wilkie, 2004)

Swash plate mechanism consists of two main parts: a stationary and a rotating swash plate (see Figure 7). Stationary part moves vertically and also tilt all directions. Rotating part rotates with the main rotor mast and is attached a stationary part by using bearing. Although it is the most mature active vibration control approach, it has some of the limitations such as: 1) high cost of implementing the HHC, 2) power which is required for actuating, 3) restrictions about the implementation HHC through a conventional swash plate due to limitation on actuation frequencies available.

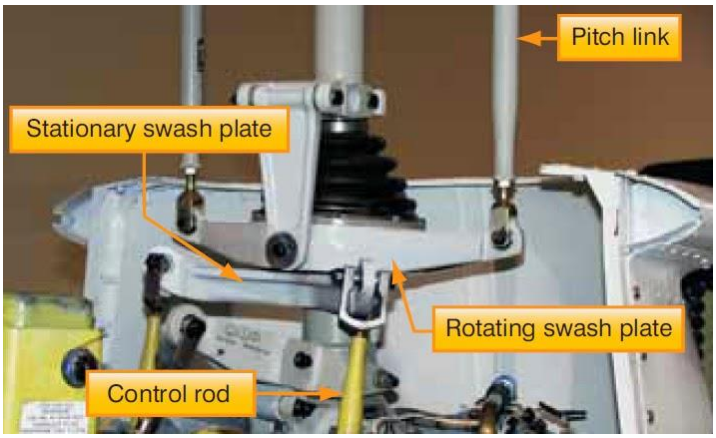

Figure 7: Swash Plate Mechanism

Individual blade control (IBC) can be seen in Figure 8 also reduces the vibration as the higher harmonic control, but IBC has a significant difference than HHC which is IBC use multiple swash plates. Using of multiple swash plates provides the more freedom for vibration control.

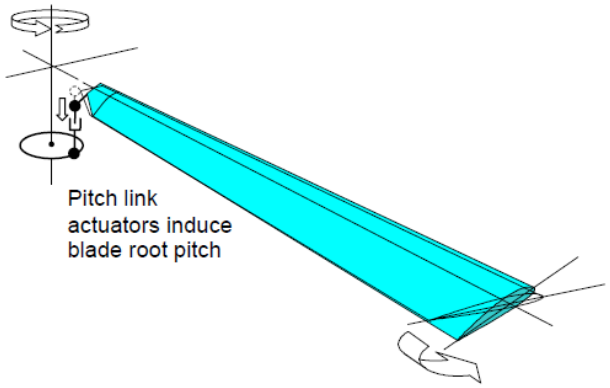

Figure 8: Individual Blade Control (Wilbur & Wilkie, 2004)

These two methods, can reduce vibration propagating from main rotor but they not a refined solution for the vibration. Furthermore, HHC and IBC have some drawback given as following;

1. There is a limited effect on reducing the vibration; due to limited actuation frequencies of traditional swash plates.
2. Applying of HHC and IBC have significant problems; hydraulic system of these complex and heavy.

3. These seems like a better way than the static control. They are more effective solution than static way but these are finite solutions because of, frameworks and structures are not capable for the unlimited working zone.

4. They only focus on the effects of vibration but cannot eliminate the source of the vibration.

"In addition, vibration reduction in rotor which controls with on-blade actuators is also widespread method. This type of reduction can give more safety and less energy consumption for the aircraft. On blade actuator's failure would not affect the flight safety as much as HHC and IBC and also consume less energy, because of on-blade actuators has not many motion part." (Sicim & Unlüsoy, 2017) Vibration control with on blade actuators are divided by two main catagory; discrete actuators which is generally known as active flap and embedded actuation.

Discrete actuators are efficient way to reduce the vibration on the structure and blades. This method uses the power of blades' aerodynamic properties. Examples of discrete actuators are active flaps, active micro flaps/tabs, leading edge slats, etc. Actively controlled flaps (ACF) performed in a single, dual or several flap arrangements are implemented between 0.6R to 0.9R along the span. (Dieterich, Enenkl, & Roth, 2006) ACF can be seen in Figure 9 reduces the vibration in the main rotor which is the significant source of the vibration helicopter. According to studies, ±4 deg flap deflection is suitable to obtain benefit without having problems with stability or performance. (Friedmann, Terlizzi, & Myrtle, 2001)

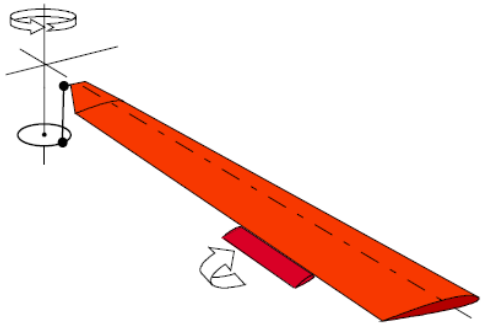

Figure 9: Active trailing-edge flap. (Wilbur & Wilkie, 2004)

The control of the aerodynamic loads acting on the blade is obtained either through changes in lift (lift effect) or by elastically twisting the blade using the pitching moment generated by the movable surface (servo-effect). In addition, discrete

actuators besides vibration reduction also are useful in improvement of performance and noise reduction. However, discrete actuators work within airfoil boundary can produce small drag and performance penalty.

The other type of the on-blade actuator method is continuous/embedded actuator. In this concept, active material is applied in the cross section of the helicopter blade. The main of the methodology is to obtain deformation by using piezoceramic layers which can induce shear strain. Embedded actuators have less profile drag when compared to the discrete actuators due to having any external moving parts like hinges or bearing. Active material being embedded inside the blade results in a maintenance cost disadvantage.

Another concept for embedded actuator is the active-twist rotor system. (Pawar & Jung, 2009) Active piezoelectric fibers which are commonly called smart materials are embedded at ±45 degree orientation on the rotor blade and they produce strain-induced twisting motions of the blade upon an applied electrical voltage difference. Numerical studies show that suitable tip twist angle is ±2 deg to achieve optimum vibration and noise reductions. (Kumar, 2013) Smart materials have some controllable properties such as stress, temperature, pH (acidity), electric or magnetic fields.

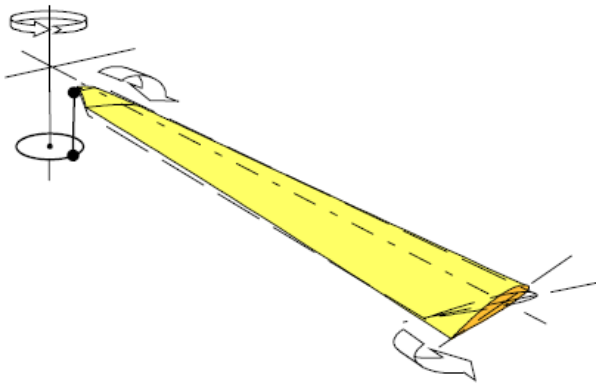

Figure 10: Active-twist rotor. (Wilbur & Wilkie, 2004)

1.3 Introduction to Piezoelectricity

Pierre and Jacques Curie performed the first experiment of piezoelectric effect on especially prepared crystals such as quartz, Rochelle salt etc. in 1880. Surface charge was made by application of mechanical stress on crystals which is known as piezoelectricity. Also, they alleged one to one correspondence between electrical effects of temperature change and mechanical stress. Although, Pierre and Jacques

Curie studied on piezoelectricity which obtains voltage when a mechanical stress is applied, the correction of opposite behaviour is proven in 1881 by Lippman. He showed that applied electric field produces mechanical stress. Name of the piezoelectricity comes from the "piezo" which means pressure in Greek language. (Boldrini, 2010)

Application of piezoelectricity can be seen in early 1900's due to the fact that it was an obscure science. Paul Langevin of France developed an ultrasonic submarine detector by the help of piezoelectricity during World War I. Piezoelectricity method used in those years's consist of thin quartz crystals sandwiched between two metal plates and provided a basis for advanced sonar devices.

At the beginning of the mid 1930's, crystal ADP (ammonium dihydrogen-phosphate) started to use to deal with limitation of production quantity and material performance. ADP was rugged as the quartz crystal and shows strong piezoelectric characteristics of Rochelle salt (Inman et al., 2000). Also, the more effective piezoelectric crystals such as EDT, DKT and BaTiO3 (Barium Titanium Oxide) were developed. With developing technology, ceramic materials produced with metaniobate (PMN) and lead zirconate titanate (PZT) which are still commonly used in today's smart material industry.

1.3.1 Piezoelectric Actuators

In this thesis, piezoelectric actuators are used to achieve active twist rotor; therefore, elaborated information is essentially given at this section. Piezoelectric materials have a mechanical flexibility and easily applicable material technology. Besides, being made of polymers and silicone lead to a low fabrication cost. Moreover, piezoelectric polymers can be utilized as active material in various transduction applications. Piezoelectric polymers have a bright future in aviation. It can be used on aircraft such as; reducing the disadvantages in airflows on the airfoils and levels of vibration on helicopters rotor blades and so on. Piezoelectric actuators can be categorized such as piezoelectric polymers, piezocomposites and voided charged polymers as seen in Figure 11.

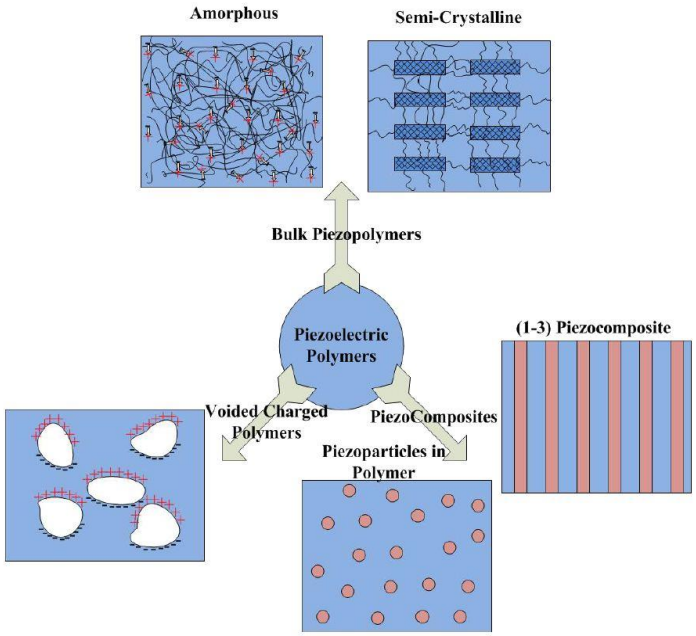

Figure 11: Piezoelectric polymer types (Ramadan, Sameoto, & Evoy, 2014)

A piezoelectric material can have an electrical field induced across its boundaries when a mechanical stress is applied on it, or vice versa. Piezoelectric material improvements start from 19th century and after that development of piezoelectric materials getting fast in first half of 20th century due to invention of MEMs and electromechanical transducers.

1.3.2 Types of piezoelectric materials

1.3.2.1 Bulk Piezoelectric Polymers

Bulk piezoelectric polymers have a piezoelectric effect because of molecular structure of the polymer and its orientation. Bulk polymers can be divided by two parts according to operating principles: the semi crystalline polymers and amorphous polymers.

Amorphous polymers are comprised of randomly organized dipoles. It is activated with influence a certain kind of electromagnetic field and temperature. Semi crystalline polymers have a semi crystalline structure such as polyvinylidene fluoride (PVDF), polyamides, liquid crystal polymers and ParyleneC. Operating principle of semi crystalline polymers is analogous with the piezoelectric materials. The theory of working statement semi crystalline polymers better clarify the concept. The positively and negatively charged ions (or polar group in polymers) are arranged in crystalline

form in semi crystalline polymers square molecular structure; they composed of positive and negative ions which are placed under compressive stresses. “For this structure, the equivalent center of charge of the positive and negative ions is still at the same point and there is no polarization change due to force applied.” (Ramadan, Sameoto, & Evoy, 2014)

1.3.2.2 Piezocomposites

A piezocomposite which is a fundamental type of smart materials is a polymer material in a embedded actuation category. Production method of piezocomposites is easier and cheaper than other smart materials because this reason, many researcher study on this issue. Two types of the piezocomposites are MFC (macro fiber composite) and AFC (active fiber composites). These two types of piezocomposites are in use at the aviation industry.

1.3.2.3 Active Fiber Composites

Active Fiber Composite was developed at MIT. AFC is an advance material to overcome the drawbacks of monolithic piezoelectric material which has an some problem with application due to brittle form. Boeing Helicopters and NASA-Langley study together with MIT in order to use AFC actuators in active vibration control. (Hagood & Rodgers, 1998) (Derham & Hagood, 1996)AFC contain piezoceramics fibers and soft polymer matrix to improve the load transfer mechanism as seen in Figure 12. Piezoceramic fibers which shows low strain behavior are inclined to crack in spite of the fact that brittle ceramic fibers provide the actuation characteristic with high stiffness. Polymer matrix applied around the fiber improved the strength properties of AFC. It takes places a path around an individual fiber for efficient load transfer mechanism. (Bent, 1997) Therefore, actuator can withstand higher strains than an individual fiber and polymer matrix prevent the crack propagation through the adjacent fibers. Polyamide film has a conductive pattern to enable the application of the driving electrical field sandwich. Interdigitated electrode pattern is used to excitation of the actuator which means an in-plane mechanical deformation in the direction of the fibers.

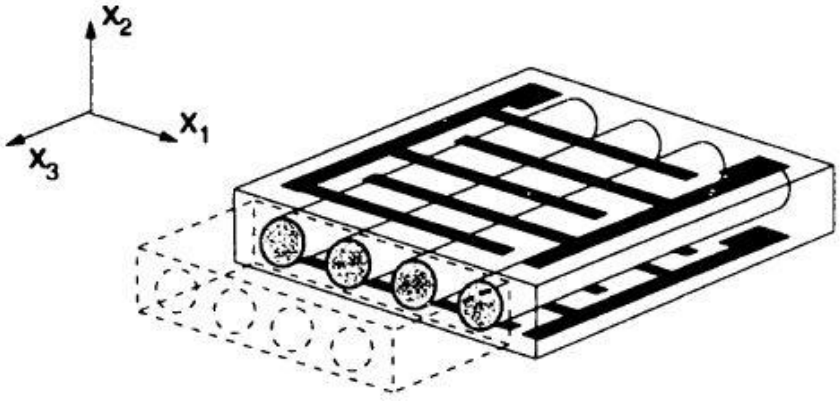

Figure 12: Active fiber composite (Bent, 1997)

1.3.2.4 Macro Fiber Composites

The Macro-Fiber Composite is an innovative material. Also, it is a low-cost piezoelectric material which is designed to control vibration, noise generation etc. (Nasa, 2017)The MFC technology try to reach adapt to environmental morphing. MFC consists of piezoelectric actuators between a two thin epoxy matrixes. By recent technology, the plates can be produced up to a total extend to 2-3 inch thick (Figure 13).

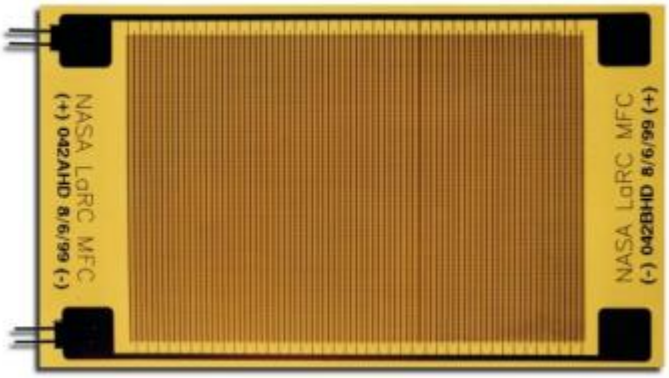

Figure 13: 3 inch MFC (Park & Kim, 2005)

Thanks to piezoelectric actuators, MFC`s can change their physical and geometric shape with the voltage change on these actuators. In general, macro fiber composites are applied between two plates and it can give a shape change to plates by means of shear, twist and traction. Moreover, MFC`s can be used as a sensor; collecting information about the state of the structure and about the applied loading. Due to this dual use, the structural health of the component can be longer than the components

without MFC. Besides all these, MFC is flexible, durable, sustainable and easy to assemble (Figure 14).

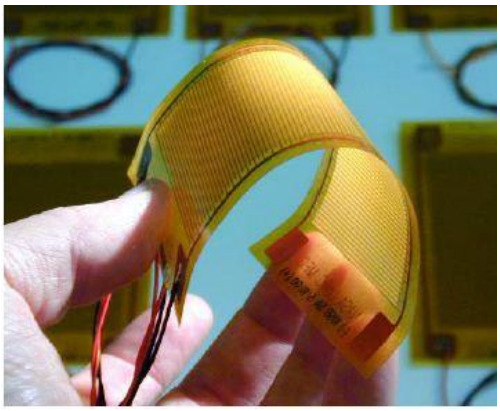

Figure 14: NASA-ARL Macro-Fiber Composite actuator. (Wilbur & Wilkie, 2004)

MFC was introduced by Wilkie as a similar material with AFC. Other piezoelectric materials were also researched by Wilkie et al. such as PNM-PT (the lead magnesium niobate-lead titanate which is used in the MFC actuators and has more free strain capacity as compared to the PZT material. William et al. introduced MFCs material properties by using classical lamination theory. Although, MFC is formed of many layers, by application of classical lamination theory, actuator is analysed as a single layer. Experimental test results show that low-amplitude response of the MFC a good agreement with the theoretical results. The response of MFC under higher stresses and excitation voltages shows nonlinearity by means of stress and strain during experimental tests. In addition, other nonlinearities are investigated by William et al.in the MFC such as nonlinear monotonic excitation and state-based hysteresis model by using data history to foresee future deflections.

The main difference between AFC and MFC is in the manufacturing process of the fiber. The MFC fibers are essentially chopped from PZT blocks. MFC is produced by machine dicing the PZT wafers. However, the AFC fibers are improved by using traditional sol-gel technique. The MFC fibers have rectangular cross-section which provide the higher PZT area per cross sectional area. Therefore, it tenders better electrical contact between the fibers. The connection of electrode pattern helps to enhance the performance of the MFCs by increasing the effective volume fraction of the fibers.

1.4 Literature Review Relevant to Thesis

Chen and Chopra (1996) develop Froude scale known as dynamically-scaled helicopter rotor blade with embedded piezoceramic elements to observe the static torsion and bending response of rectangular beams and rotor blade. (Chen & Chopra, 1996)A 6 ft diameter 2-bladed bearingless rotor is designed with NACA 0012 cross-section. Piezoelectric actuators are embedded at ± 45 degree angles on the top and bottom surfaces. A bending distribution is obtained through out-of-phase excitation of the top and bottom actuators by applying same potentials. In addition, a twist distribution through the blade span is succeed in-phase excitation. A uniform strain beam theory is used to fix design variables and to optimize blade performance. The analytical model results for static bending and torsional response of the rotor blade are compared with experimental data. The study shows that uniform strain theory can be used to predict trends of torsion and bending response of the rectangular beam. Also, static torsion response can be estimated by using uniform strain theory with an accuracy of %80. (Chen & Chopra, 1996)

DLR (Deutsches Zentrum für Luft- und Raumfahrt e.V.) has some research about the active twist blades concept. During the research, different geometrical shapes and different design processes are applied. In addition, the blades power consumption for noise and vibration reduction is compared for different designs. A unique testing technique is given for non-destructive measurement of mass distribution. DLR focus on principle of shear introduction by helping piezoelectric actuators. BO-105 model rotor blade is a baseline of the blade characteristics which occurs C-Spar which is made of unidirectional glass fiber, a glass fiber skin and a foam core. The chord length equals 0,121 meters and the radius is 2 meters. NASA developed Macro Fiber Composites (MFC) used in this study. The operational voltage of these type of actuators are between -500 V and +1500V to provide a sufficient electrical field. (Monner, Riemenschneider, Opitz, & Schulz, 2011) Blade models built in DLR are given as following with active area, fiber angle and actuator angle:

	Airfoil	Active Area	Fiber Angle	Actuator Angle
AT1	NACA0012	1075cm²	-30	45
AT2	NACA0012	1600 cm²	-30	40
AT3	NACA23012/OA209	2150cm²	+-45°	45
AT4	NACA23012	1275cm²	+-45°	45°
AT5	NACA23012	2225cm²	+60°	-50°

Figure 15: DLR Active Rotor Blades AT1 through AT5. (Monner, Riemenschneider, Opitz, & Schulz, 2011)

Other recent study conducted by Sekula, Wilbur and Yeager (2004) focus on how blade geometry can be changed to increase the blade active twist control and to reduce unactuated rotor vibration. To reach these aims, five studies are examined. The first study is conducted to learn how blade geometry influences the blade torsion response which affects the blade active twist. The goal of the other four studies is to show the impact of various blade geometry parameters on hub vibration by using different advance ratios. During the studies, blade structural properties are assumed to be independent of the blade geometry properties and also assumed constant along the blade span. The results of the models show that increasing the twist in low-speed flight decrease the hub vibration and for cruise and high-speed flight -10^{o} of twist can be minimized the nose down twist which reduce the hub vibration. (Sekula, Wilbur, & Yeager, 2004)

Gluhihs and Kovalovs (2006) decide to investigate a helicopter blade with surface-bonded actuators under loading. The helicopter blade is modelled as an aluminium plate by using SHELL99 element which is suitable for layered applications of a structural shell model in ANSYS. Simple thermoelastic analogy is used to apply the voltage effects. An aluminium plate with geometrical parameters length L = 4.0 m, width B = 0.2 m, and thickness t = 0.025 m is modelled. The plate is divided into 10 equal parts as seen Figure 15. q = q0×sin (wt) is assumed harmonic plane pressure

load and it creates twisting moment. The constant structural damping ratio is assumed to be 0.01.

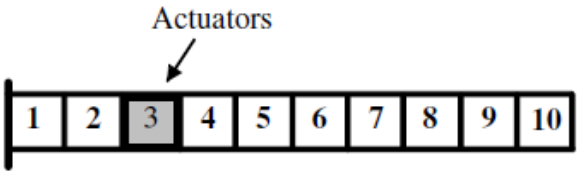

Figure 16: Illustration of an aluminium plate with PZT pairs for position 3. (Kovalovs & Gluhihs, 2006)

The results for four twist mode shapes is given in Figure 16 with frequencies f of 48.0, 141.6, 237.0, and 338.4 Hz. Reduction in vibration and optimum voltages are obtained and maximum ratio of reduction/optimum voltage gives the optimum position of actuators.

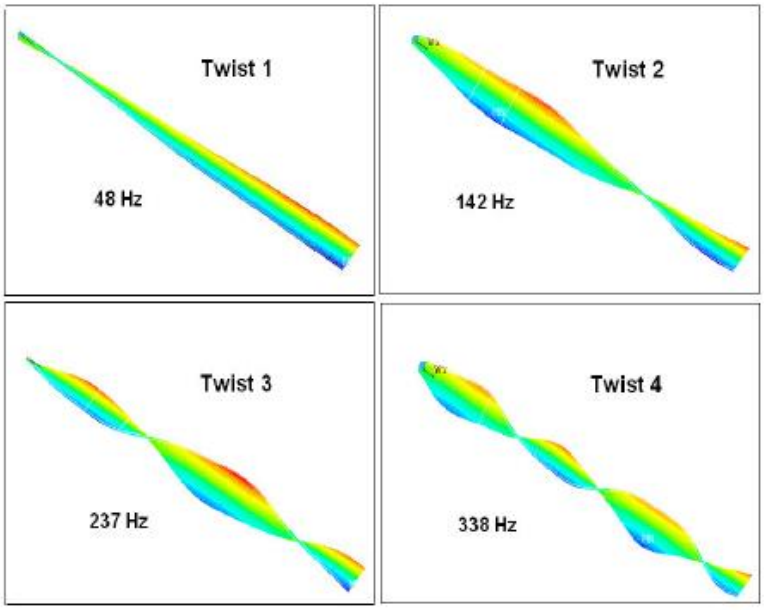

Figure 17: Twist mode shapes of an aluminium plate with piezoelectric actuators. (Kovalovs & Gluhihs, 2006)

The results are given in thesis by the tables which show the optimum positions of actuators according to maximal ratio reduction/optimal voltage for each twist mode shapes. Also, the effect of the geometric dimensions on the control of plates was studied. According to obtained results, increasing in the number of bonded piezoelectric actuators can be decrease the optimal voltage for all four twists modes. Gluhihs and Kovalovs conclude that the optimum placement of actuators depends on

the form of twist modes and the length of piezoelectric actuators affects the active control of plates. (Kovalovs & Gluhihs, 2006)

Kovalovs, Barkanov and Gluhihs (2007) continue their research with development of an active twist actuation concept by using macro fiber composite (MFC) actuators. MFC actuator includes polyamide films with IDE-electrodes. Their orientation is at ±45 degrees of angle to the spar axis of the rotor blade. They are glued on the top and the bottom of piezoceramic ribbons. MFC actuators induce shear stresses based on the properties and the orientation of piezoelectric actuators so this causes the twisting movement along the blade. Helicopter rotor blade is investigated by using NACA 23012. The blade has a rectangular shape, active part radius equals to R= 1.56 m and chord length is c=0.121 m (Figure 18)

D-spar is used on rotor blade with unidirectional Fiberglass Reinforced Polymer skin made of +45% - 45% GFRP, a foam core, MFC actuators

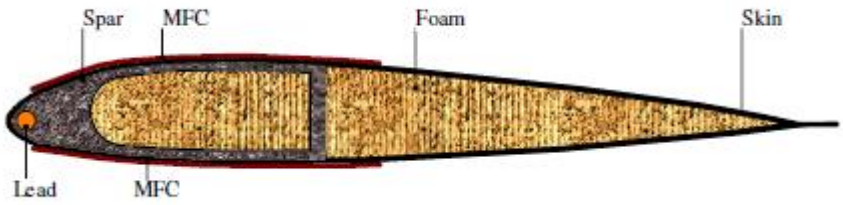

Figure 18: Cross-section of the helicopter rotor blade. (Kovalovs, Barkanov, & Gluhihs, 2007)

The 3-D finite model is produced by ANSYS. Electric field is modelled as a thermal load and the relationship between the piezoelectric strain and thermal strain is given as:

$$\alpha_{ij} = \frac{d_{ij}}{\Delta_{ES}}$$

where d_{ij} is the effective piezoelectric constant and Δ_{ES} is the electrode spacing taken as Δ_{ES}=0.5 mm. During this study, optimum placement of actuators in helicopter rotor blades is determined by using the finite element method on the parametric study results. From the optimisation results after the compare with previous results, it can be inferred that 'the 2nd variant arrangement of MFC is more effective than the 1st in the production of a maximum torsion angle under voltage on 26 %. (Kovalovs, Barkanov,

& Gluhihs, Numerical optimization of helicopter rotor blade design for active twist control, 2007)

Wiciak and Trojanowski (2014) study on effects of different shapes and material composition of piezoelectric actuators on the vibration reduction. For this aim, four numerical models which have two piezoelectric elements are used. For each model, first piezoelectric elements used for plate excitation are the same shape and same composition. To reduce the vibration, the second elements which have different shape and material compositions are used. Numerical models are created by using ANSYS software (Figure 19).

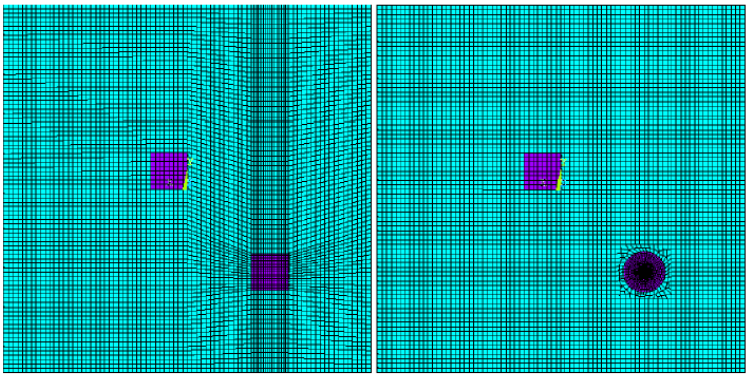

Figure 19: Created Models. (Wiciak & Trojanowski, 2014)

The first element is common for each model and has a square homogeneous shape. The other elements which are the most important due to vibration reduction have different shapes and compositions (Figure 20).

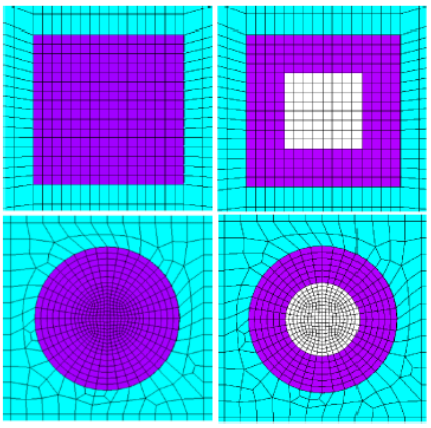

Figure 20: Different shape and composition of second element. (Wiciak & Trojanowski, 2014)

In Figure 20, left column shows homoheneoud elements and the right column show elements which have two parts.

- Square shape – homogeneous element, a= 40 mm and h=1 mm
- Circle shape- homogeneous element, r= 40/π mm and h=1 mm
- Two part square element, a=40 mm and h=1 mm (The outer area equals to 4 times of inner area)
- Two part circle element, r= 40/π mm and h=1 mm (The outer area equals to 4 times of inner area)

According to performed simulations, different composition square shape elements don't cause significant difference. Homogeneous and two parts elements have nearly same effects. In addition, results for circle elements have the same situation and the differences between results are even smaller than square shapes results. The research shows that vibration reduction isn't influenced significantly with the change in composition of piezo elements. (Wiciak & Trojanowski, 2014)

CHAPTER 2

DESIGN OF ACTIVE TWIST ROTOR BLADE

2.1 Geometry and Mesh Modeling

The main goal of this chapter is to make an emphasis on the design of the active twist rotor blade which smart materials are intended to be installed to initiate a twisting motion. Shark-120 helicopter which is a model of unmenned systems developed by Oneseen Skytech. It is used as a baseline characterictic of blade design in this study. Shark-120 unmanned helicopter has a real-time aerial monitoring system (RAMS). Appearance and specification of the Shark-120 helicopter can be seen in Figure 21 and Table 1. Shark-120 is a gasoline-powered unmanned helicopter of conventional helicopter layout. The landing gear system consists of a pair of skids and the UAV is fully autonomous.

Figure 21: Unmanned Helicopter. (Choi , Lee , Lee , & Kim , 2012)

Table 1: Specifications of the Shark-120. (Choi , Lee , Lee , & Kim , 2012)

Main Rotor	4 Rotor
Motor	294 cc, 6500 rpm
Weight	83 kg
Payload	40 kg
Operational Range	15 km
Flight Time	1 hour
Speed	40 km/h
Main rotor diameter	3.12 m
Length	2.86 m
Width	0.75 m
Height	1.18 m

Geometry of rotor blade is modeled as mostly 3-D geometry. Base foam and D-Spar are modeled with 3-D elements. Skin and solid patch are modeled as 2-D layered section using ANSYS. Rotor blade can be shown in Figure 22 is designed with NACA23012 airfoil Blade radiues equals to 1.56 m and chord length dimension is 0.121 m. Also, it has a rectangular shape with radius. The basic design parameters such as airfoil section, wing planform area S, wing chord length c, wing span b, aspect ratio A and thickness to chord ratio t/c are determined at design process. Figure 22 and Table 2 show details of these parameters for the rotor blade design.

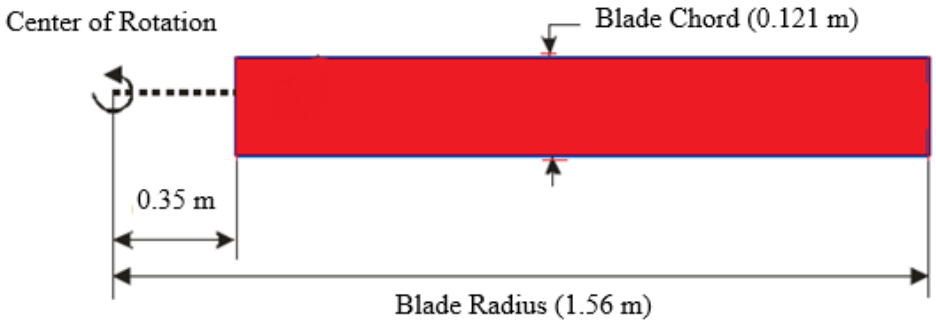

Figure 22: Rotor Blade Conceptual Design Geometric Parameters (SI Units).

Table 2: Rotor Blade Conceptual Design Geometric Parameters (SI Units).

Airfoil Section	NACA 23012
Thickness, t	14.8
Chord Length, c	122.6
Thickness to Chord Ratio, t/c	0.14

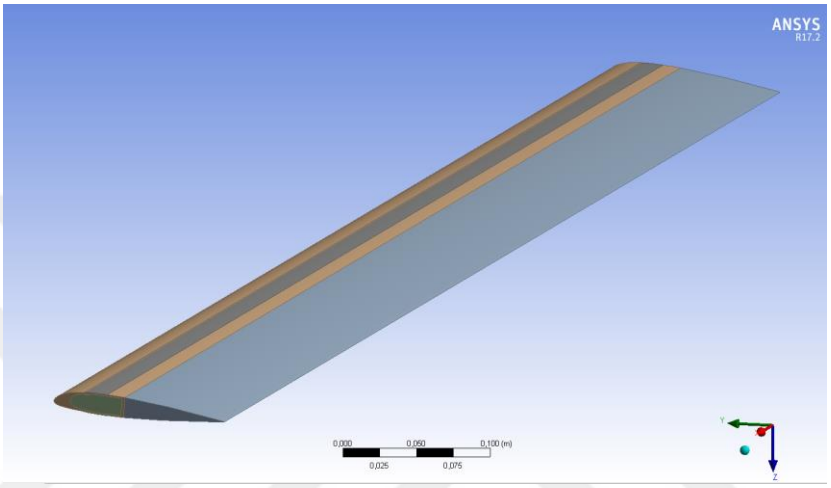

Figure 23: Isometric View of the helicopter rotor blade 1

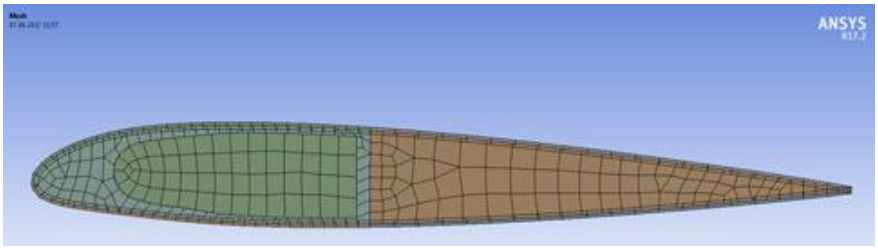

Figure 24: Isometric View of the helicopter rotor blade 2

D-spar is used to increase strength of the blade. The material of the D-spar is unidirectional Glass Fiber Reinforced Polymer (GFRP). Also it consists of MFC actuator and skin made of $+45^0/-45^0$ GFRP. MFC actuators consist of piezoceramic fiber and sandwiched between polyamide films that have attached interdigitated electrode patterns. Thickness of each skin GFRP layer equals to 0.125 mm

For material property assignment, GFRP (Glass Fiber Reinforced Polymer) and foam materials are defined at workbench database. D-Spar GFRP material is assigned unidirectionally. Material properties are given in Table 2.2 and Table 3:

Table 3: Properties of materials used in the cross-section. (Sicim & Unlüsoy, 2017)

	Glass Fiber Reinforced Polymer (GFRP)	Foam	MFC
E_X	45.166 GPa	0.035 GPa	15.5 GPa
E_Y	11.981 GPa	0.035 GPa	15.5 GPa
E_Z	11.981 GPa	0.035 GPa	30.0 GPa
Gxz	4.583 GPa	0.014 GPa	5.7 GPa,
Gyz	1.289 GPa	0.014 GPa	10.7 GPa,
Gxy	1.289 GPa	0.014 GPa	10.7 GPa
υ*yz*	0.325	0.25	0.35
υ*xz*	0.238	0.25	0.4
υ*xy*	0.238	0.25	0.4
ρ	2008 kg/m3	52 kg/m3	4700 kg/m3

Structure of blade contains two different materials. Main load carrying D-spar and skin of blade made of Glass Fiber Reinforced Polymer. Inner part of D-spar and rear side of D-spar made of Foam due to weight considerations. Foam parts can be seen at Figure 25.

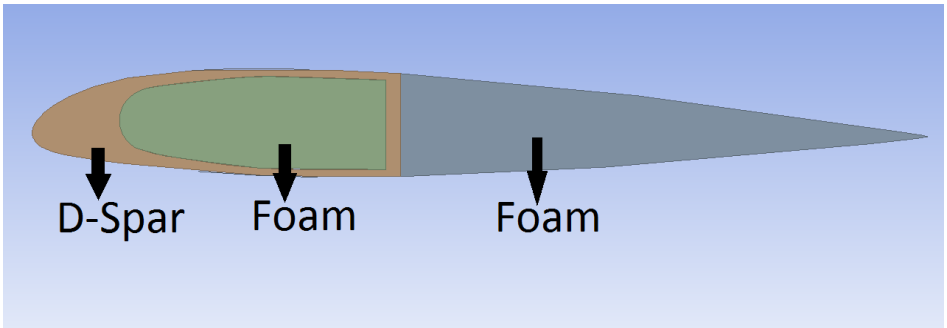

Figure 25: Cross-section of blade

Due to skin of blade being too thin, skin constructed with areas so that finite element model can be created with shell elements. All parts of blade except the skin are modeled by using quadrilateral (SOLID186) elements. Since the thickness of the blade skin and thickness of the solid patch are considerably small, they considered to obey the thin walled structure theory. While modeling skin and solid patch, layered section feature of ANSYS is employed with SHELL181 element. Thicknesses and layer

orientations are given as inputs of Layered-Section Menu of ANSYS as seen at Figure 26 and program generated skin layers automatically. Also, total thickness of skin is 0,001 m as it can be seen in Figure 26.

Layer	Material	Thickness (m)	Angle (°)
(+Z)			
8	GFRP	0,000125	45
7	GFRP	0,000125	-45
6	GFRP	0,000125	45
5	GFRP	0,000125	-45
4	GFRP	0,000125	45
3	GFRP	0,000125	-45
2	GFRP	0,000125	45
1	GFRP	0,000125	-45
(-Z)			

Figure 26: Layer thickness and orientation of blade skin

Initially, blade is separated into 10 discrete sections to make finite element modeling easier. Due to hub of blade not being modelled, root of the blade starts at 0,35 m and blades completes at 1,56 m and hub center point is taken as [0,0,0] while modeling as can be seen at figure.

Figure 27: Top view of blade

Model is divided into several equidistant parts to make meshing easier. All mesh structures are generated from quad elements. Details of mesh, MFC patch and skin can be seen at Figure 28.

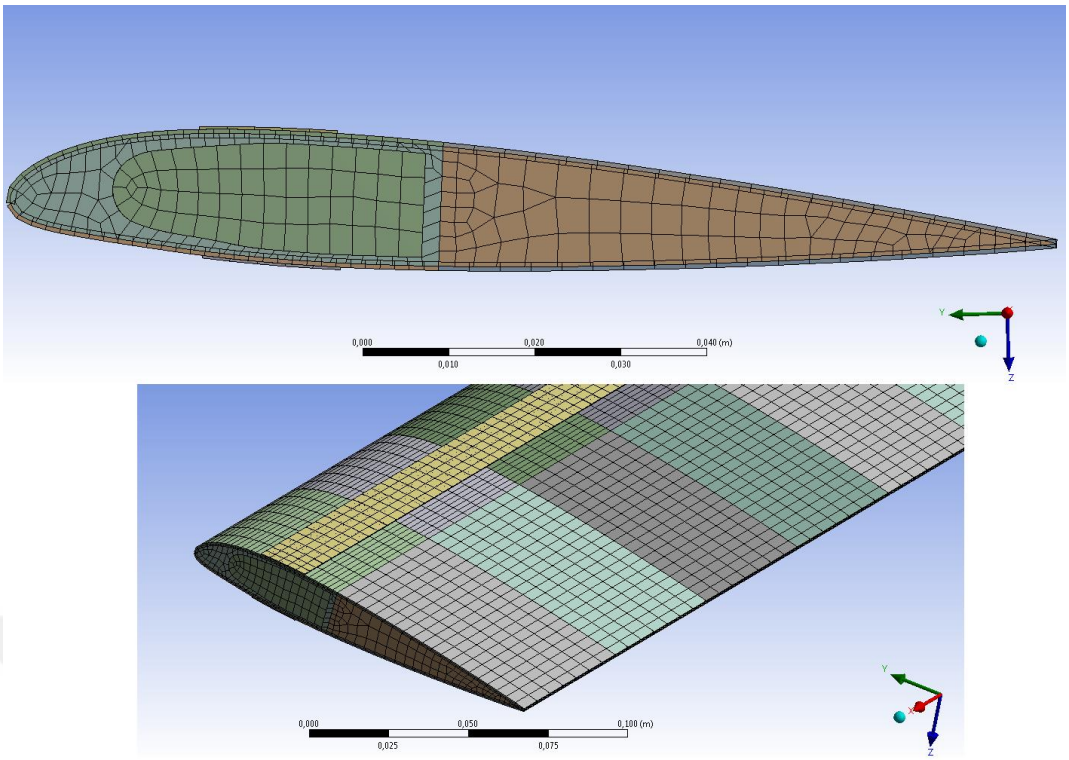

Figure 28: Mesh details of FE Model

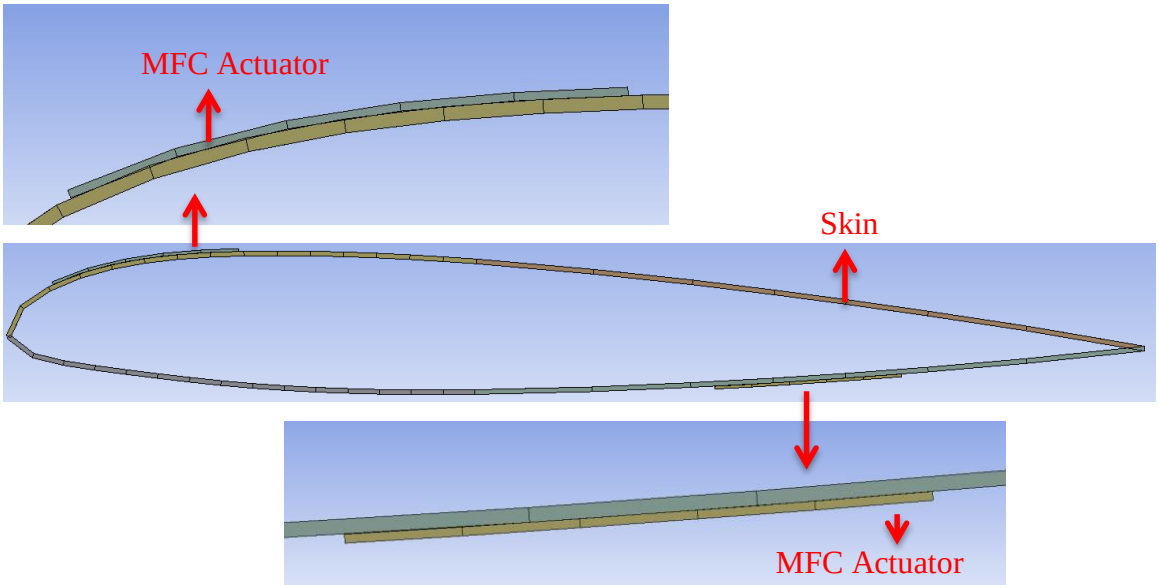

Figure 29: Mesh details of FE Model

There are total of 38775 elements and 137559 nodes generated for FEM. FE model details of parts are given at .

Table 4: FE model details of parts

Element Type: SOLID186	**#of Elements**	**# of Nodes**
D-Spar	8300	50663
Skin	14000	14100
MFC Patch	1975	2382
Foam	14500	73031
Total	38775	137559

Note that summation of nodes is not match with total number, because of neighbor elements share nodes between D-spar and Foam etc.

2.2 Finite Element Modeling of Rotor Blade

2.2.1 Analysis Types Used on This Study

In this section, analysis type which are used in theses and flow cart related to analysis steps are given. Analyses start with Fluent CFD analysis and continue with the ANSYS FEM analysis which leads a one way fluid-structure interation analysis. Figure 30 shows the details and steps of the analysis process.

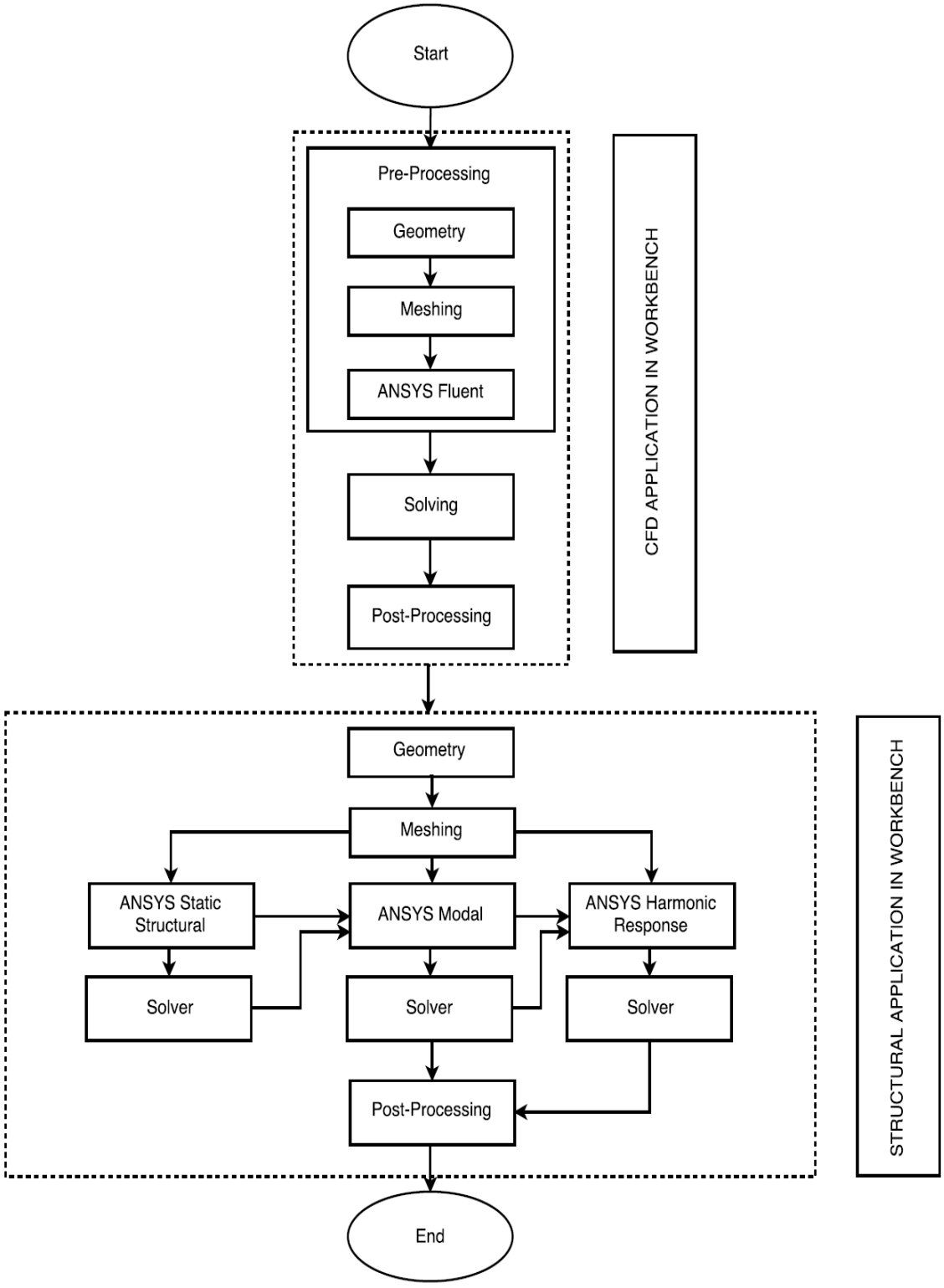

Figure 30: Flow chart of general analysis steps

2.2.1.1 Static Analysis

Static structural shows stresses,strains and displacements. Also, it shows the forces applied in structure and components of loads in 3D dimention. This type of analysis can be conducted by ANSYS, Samcef, or ABAQUS solver. The loading type applied in static analysis can be seen as following: external forces, pressures, temperature and steady-state inertial forces.

2.2.1.2 Modal Analysis

Modal analysis are used to obtain vibration characteristics of structure. The results of this analysis use in in a downstream dynamic simulation employing mode-superposition methods, such as a harmonic response analysis, a random vibration analysis. Main results of the analysis are natural frequencies and mode shapes.

2.2.1.3 Harmonic Analysis

"In a structural system, any sustained cyclic load will produce a sustained cyclic (harmonic) response. Harmonic analysis results are used to determine the steady-state response of a linear structure to loads that vary sinusoidally (harmonically) with time, thus enabling you to verify whether or not your designs will successfully overcome resonance, fatigue, and other harmful effects of forced vibrations. This analysis technique calculates only the steady-state, forced vibrations of a structure, typically at a number of discrete points within a range of frequencies. The transient vibrations, which occur at the beginning of the excitation, are not accounted for in a harmonic response analysis." (ANSYS® Academic Research Release)

2.2.1.4 CFD Analysis

Computational fluid dynamics analysis shows fluid flow analysis of incompressible and compressible fluid flow and heat transfer in different compact geometries. Fluent and also CFX is used as a tool for CFD analysis. In this study Fluent is used to define mathematical models (e.g., low-speed, high-speed, laminar, turbulent, etc.),to select materials and to define boundary conditions.

2.2.1.5 Fluid-Structure Interaction

Fluid-Structure Interaction (FSI) analysis is used to define the relationship between fluid and solid structure. FSI analysis includes mechanical application which

has interaction with corresponding fluid. There are two different FSI analysis which are named as one-way FSI and two-way FSI.

One-way FSI: The result from a CFD analysis at the fluid-structure interface is applied as a load to the Mechanical application analysis. The boundary displacement from the Mechanical application is not passed back to the CFD analysis.

Two-way FSI: Structural analysis results are transferred to in the Mechanical application are transferred to the CFD analysis as a load in this analysis type. Similarly the results of the CFD analysis are passed back to the Mechanical application analysis as a load.

2.2.2 MFC Patch

"Significant vibration and noise reduction can be achieved without the need for complex mechanisms in the rotating system using active twist control of helicopter rotor blades by the application of MFC actuators. In this case MFC actuators are implemented in the form of active plies within the composite skin of the rotor blade with orientation at 45 to the blade axis to maximize the shear deformations in the laminated skin producing a distributed twisting moment along the blade." (Kovalovs & Gluhihs, 2007)

2.2.3 CFD Modeling and Setup in ANSYS Fluent

2.2.3.1 Pre-Processing

In this thesis study, ANSYS Fluent 17.2 version is chosen for CFD solver. ANSYS is launched from the Workbench utility which allows the user to set up a case step-by-step in an ordered procedure.

In order to couple prerequisite for fluid-structure interaction, location of blade has to identical for both structural and fluid models. To satisfy this condition after blade geometry is generated, fluid domain is generated on top blade geometry and blade geometry is suppressed in FLUENT before mesh operation. Two fluid domains are constructed during CFD analysis. First one is near blade region with fine mesh and second one is far from blade with coarser mesh considering computational cost. Domains which are mention as below can be seen in Figure 31 to Figure 33.

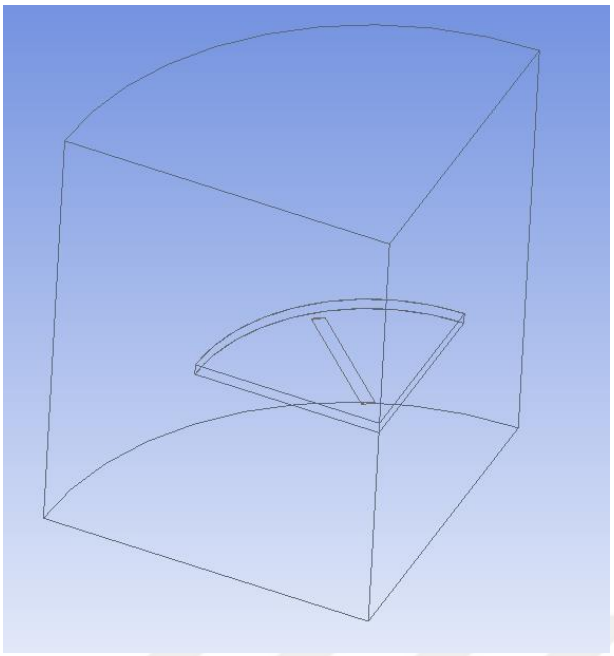

Figure 31: Full CFD Domain

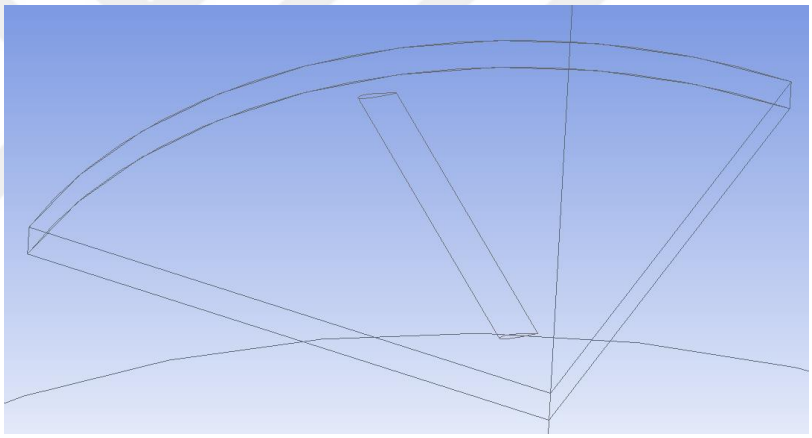

Figure 32: Near Blade CFD Domain

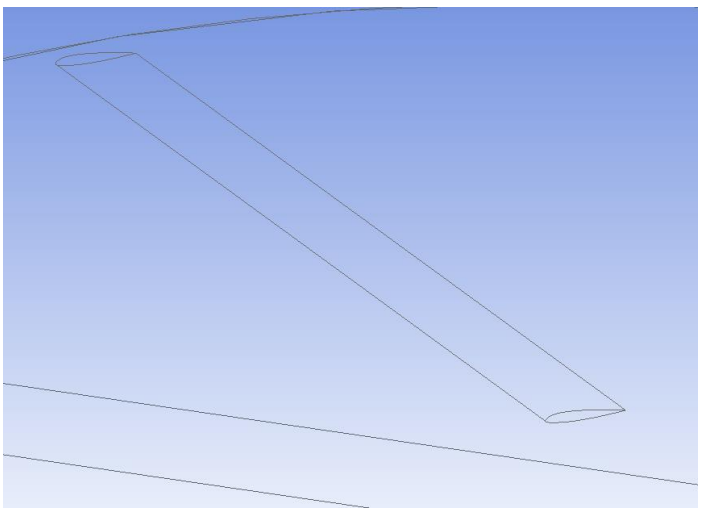

Figure 33:Blade inside Fluid Domains

2.2.3.2 Domain Decomposition

As it was previously stated, the domain was simplified to a 90° circular. The helicopter rotor is considered for this project has four blades; hence the domain is one fourth of a full 360° domain that could be modeled for the entire rotor. Moreover, the mesh is composed of different named selections in ANSYS Meshing which correspond to the boundary conditions that will be implemented in ANSYS Fluent. These named selections allow for the naming of the faces of the mesh to be recognized with a specific name and to be automatically assigned to the specified condition in ANSYS Fluent such as wall conditions or periodic boundary. General view of flow mesh can be seen in the Figure 34.

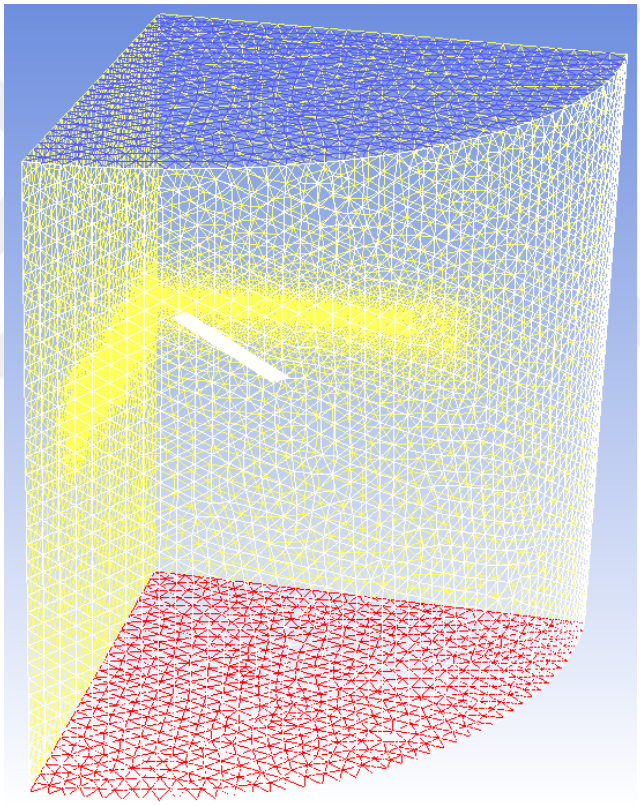

Figure 34: General view of CFD mesh

2.3 Application of the Boundary Conditions

2.3.1 Structural Boundary Conditions in ANSYS Mechanical

2.3.1.1 Static Structural Analysis Boundary Conditions

At the beginning of the modeling, patch locations should be determined. In order to determine these locations, an iterative process is performed. According to

different application area, MFC material embedded both upper and lower skin to obtained optimum twist motion.

Patch is applied to certain locations on the model and only voltage load is applied to model to solely trigger the MFC patch. After locations are set for MFC patch, model is fixed from global coordinates of [0, 0, 0], which is taken as rotor hub point, with help of constraint equations that can be seen from Figure 35.

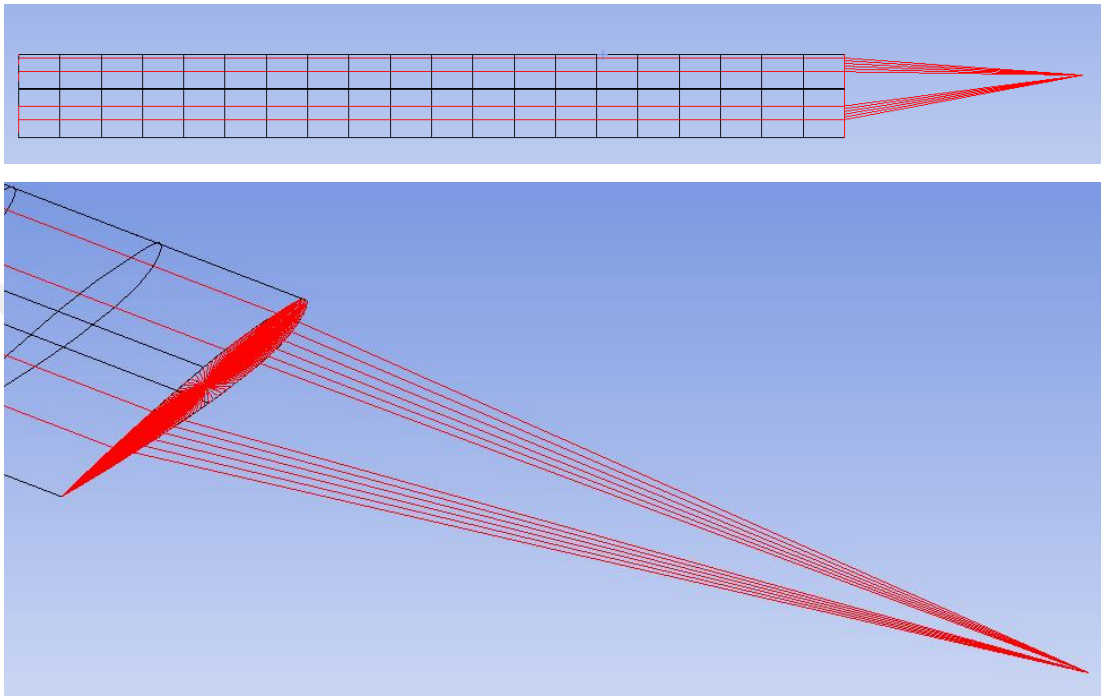

Figure 35: Constraint defined to FE model

After that, CFD load is transferred to model from FLUENT and rotational velocity of 1800 RPM is defined to model. Location of rotational velocity and direction is seen in Figure 36.

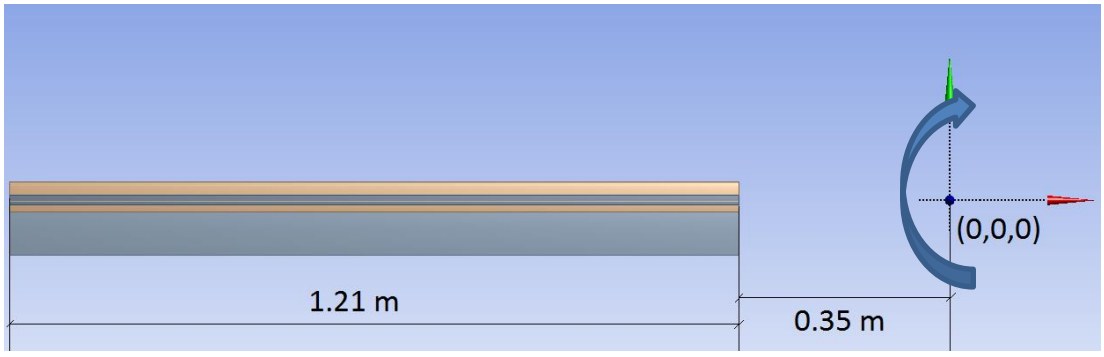

Figure 36: Rotational velocity defined to FE model

After model is set, MFC input load is defined to model. Note that, from modeling approach voltage is given as temperature input and thermal expansion is

considered as simulation of MFC patch's behavior. This approach is explained in section 2.3.1.4 which is related to patch boundary conditions. For each parameter, all analyses begins with static structural model to taken into account MFC patch's behavior and update stiffness of model before solving pre-stressed modal analysis.

2.3.1.2 Modal Analysis Boundary Conditions

The modal analysis of design is performed by default solver type for modal analysis in workbench mechanical. Before performing analysis, all six degrees of freedom of the root nodes are fixed as shown at Figure 37.

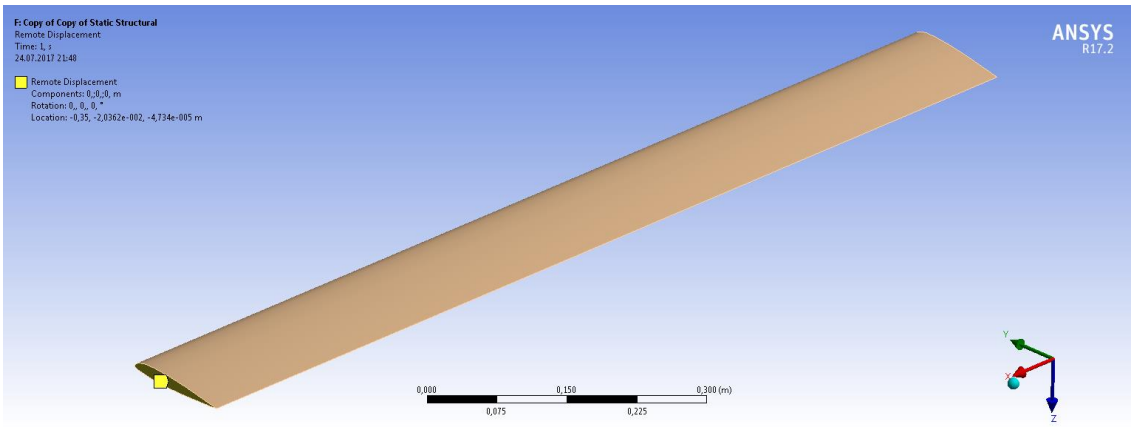

Figure 37: Degree of freedom of the root nodes

Knowing that blade rotates at 1800 rpm, blade rotation needs to be taken into account in modal analysis. Therefore, Pre-Stressed Modal Analysis is performed to considered effects of rpm load on frequencies and mode shapes. Aim of the model analysis is to determine the torsional mode frequencies of blade and acquisition of knowledge prior to harmonic analysis. Results of analysis before MFC applied can be seen Table 5. 1st torsional mode is found at 5th mode. Therefore, this study is concentrated on 5th mode of the blade. Detailed results can be seen in Appendix A for various results including before and after MFC applied for different loads.

2.3.1.3 Harmonic Analysis Boundary Conditions

The harmonic analysis of design is performed using default solver type which is defined in ANSYS. A modal analysis performed before harmonic analysis in order to obtain 1st torsional modes frequency. Then, analysis time steps of harmonic analysis are defined accordingly. Before performing analysis, all six degrees of freedom of the

root nodes are fixed as shown at Figure 37. Aerodynamic loads are calculated from a separate analysis and applied to model as pressure loads are given on blade skin through FSI interaction. Also, rotational velocity of 1800 rpm is given to model. Aim of the model is observing maximum angular deformation on blade and determining the location and magnitude of deformation on torsional mode. Detailed results and comparison of models after patch applied are given at results section.

2.3.1.4 Patch Boundary Conditions

Application of MFC on Finite Element Analyses is quite simplified. Input of MFC actuators are given as thermal loads. Relation between thermal strain and piezoelectric strain is given as;

$$\alpha_{ij} = \frac{d_{ij}}{\Delta_{ES}}$$

d_{ij} term stands for piezoelectric constant. During modeling voltage, temperature analogy is used. Applied temperature is assumed to equal to given voltage. (Ben-Zeev & Chopra, 1995)

$$V \sim \Delta T$$

Position of patch is determined with an iterative procedure. Flow chart of procedure is given below figure. (Centolanza, Smith, & Munsky, 2002)

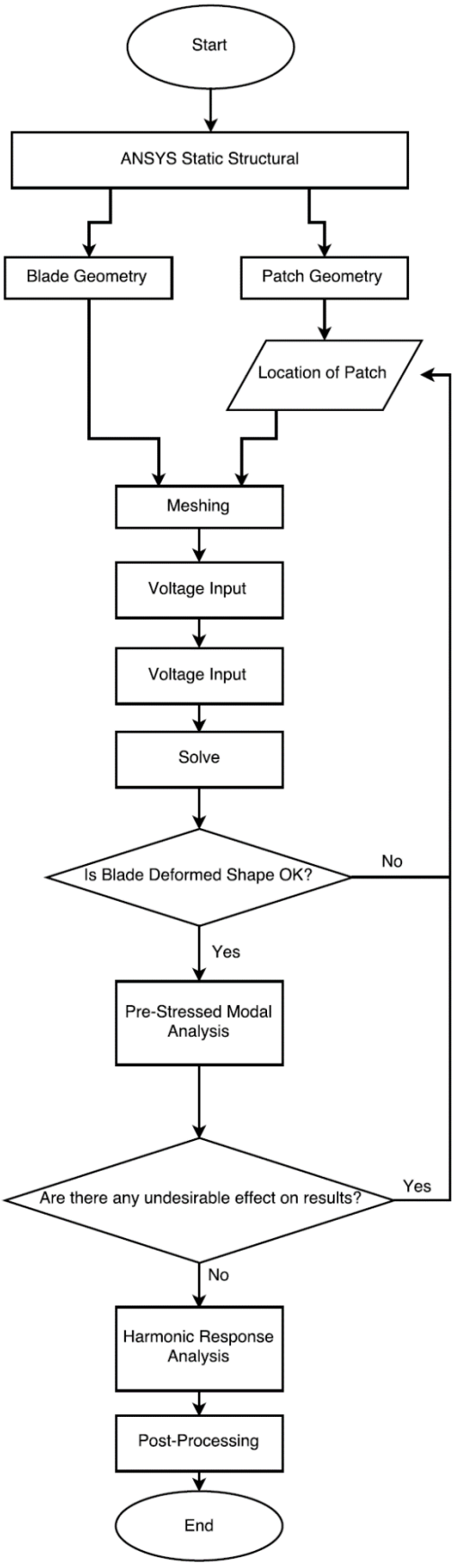

Figure 38: Flow chart of MFC Patch Positioning

2.3.1.5 Fluid Boundary Conditions in ANSYS Fluent

The boundary conditions for the CFD model are set up as seen figure below. Set up the model in Fluent given that this type of simulation can be exceptionally challenging. The model does not only involve the air flow conditions, but also periodicity and rotational machinery capabilities in order to correctly replicate the actual behaviour of the helicopter rotor blades.

The named selections for the inlet and outlet boundary conditions in ANSYS Fluent given as below.

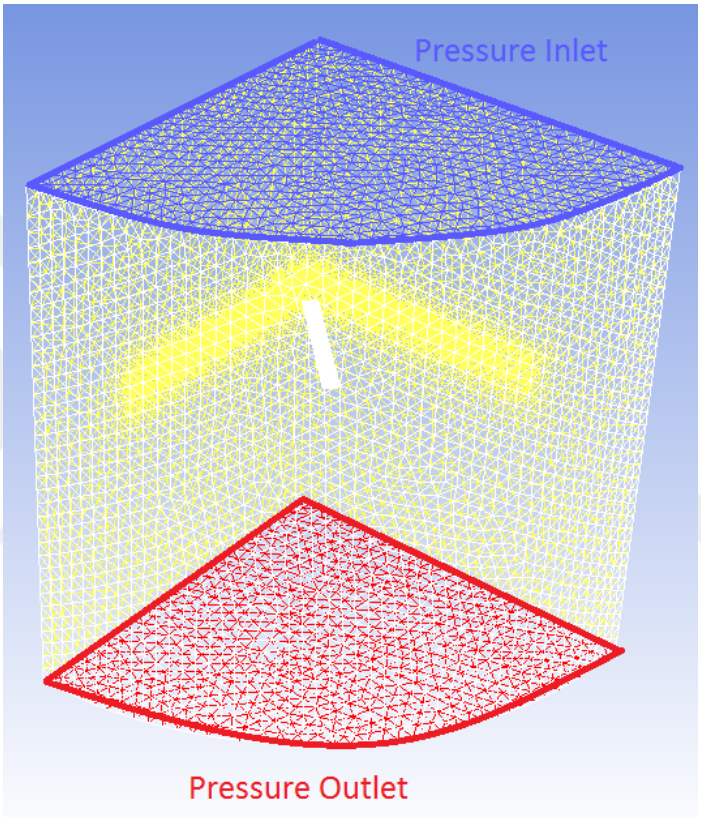

Figure 39: Boundary conditions in Fluent

The following image also shows the boundary conditions for the blades. As it can be seen, only the surface mesh of the blade is considered as being defined as a wall in the model given and the geometry of the blade was suppressed from the rest of the domain.

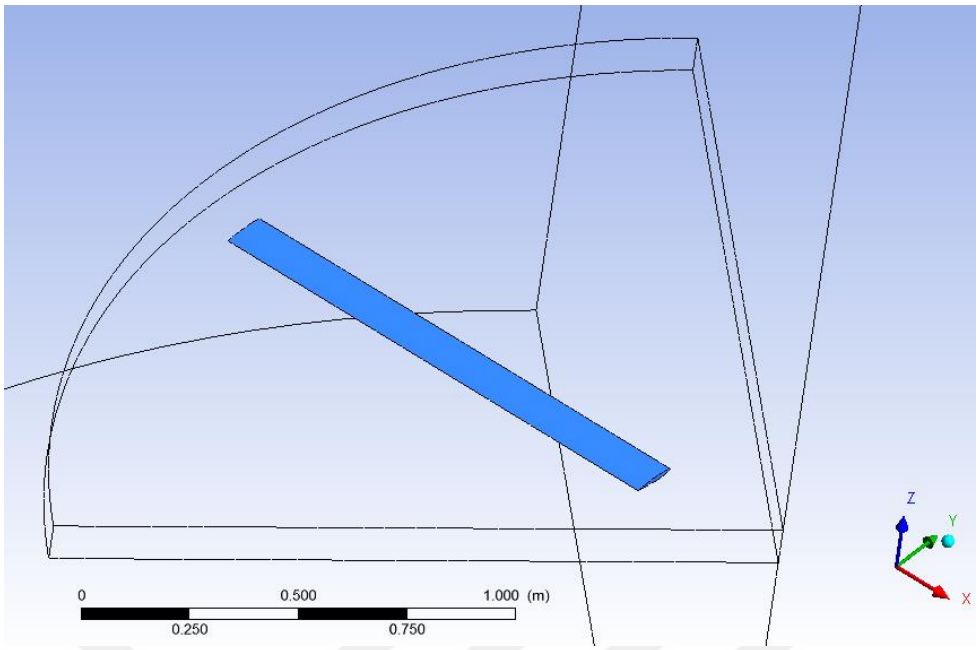

Figure 40: Boundary condition in Fluent for blade section

ANSYS Fluent can model fluid flow in complex geometries. Unlike other software used for rotating blade analyses (such as BEM based software), it does not need to use predetermined airfoil data for the prediction of the fluid flow, but instead it solves for the governing continuity equations at thousands or millions of positions, depending on the mesh density, on and around the blade in an iterative process. All the velocities, including the span wise velocity are considered. Moreover, the results obtained from CFD solvers such as Fluent are more realistic and precise than any codes generated based on BEM theory.

As it was specified before, the whole domain was a fourth of a horizontally placed conic frustum with only one blade inside, as shown in Figure 42 Each side of the domain was given periodic boundary conditions. When periodic boundary conditions are used, it implied that the velocities going out of a shadow boundary (left symmetry boundary) can enter the boundary on the other side in an infinite loop. Figure 42 illustrates a typical application of periodic boundary conditions. In this example, the flow entering the computational model through one periodic plane is identical to the flow exiting the domain through the opposite periodic plane.

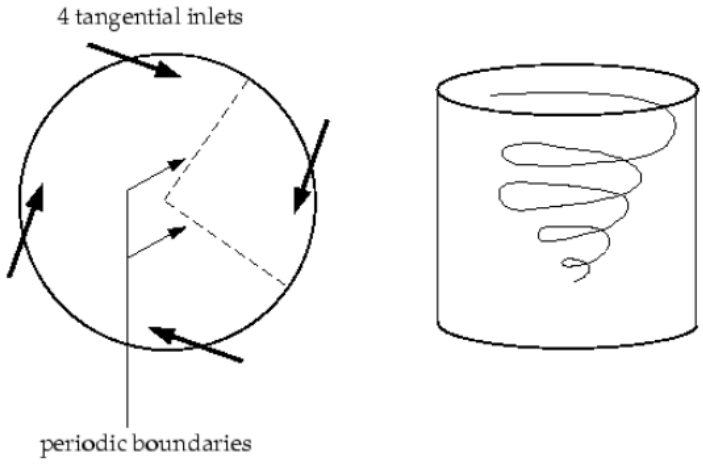

Figure 41: Periodic Boundaries to Use defining Swirling Flow

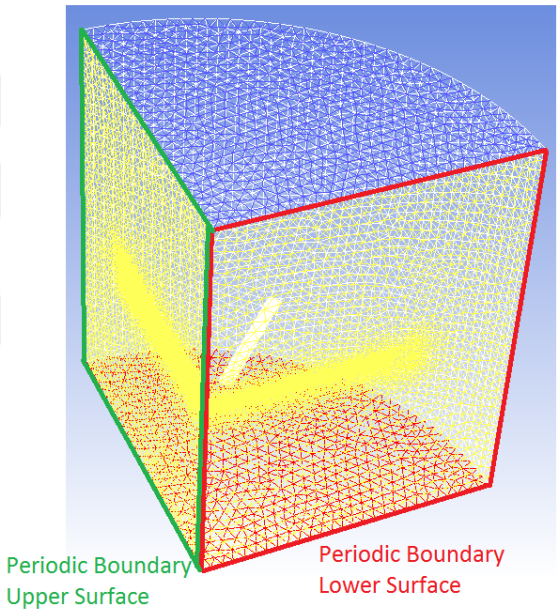

Figure 42: Periodic boundary surfaces in Fluent

For solver, density based solver is choosen in steady state condition. Energy equations are turned on and k-omega model with SST model is preffered for viscous model. Angular velocity of 1800 RPM defined to blade in cell zone conditions.

2.3.2 Fluid-Structure Interaction Modeling

Having both structural and fluid analyses in this study, best option was using Fluid-Structure Interaction (FSI) modeling. To achieve a successful interaction, both blade geometry and location of blade in fluid domain have to have identical position in space. Afterwards, using workbench environment, result file of CFD analysis link

to setup of structural analysis as seen in Figure 43. Using this link, CFD loads are transferred to structural analysis automatically.

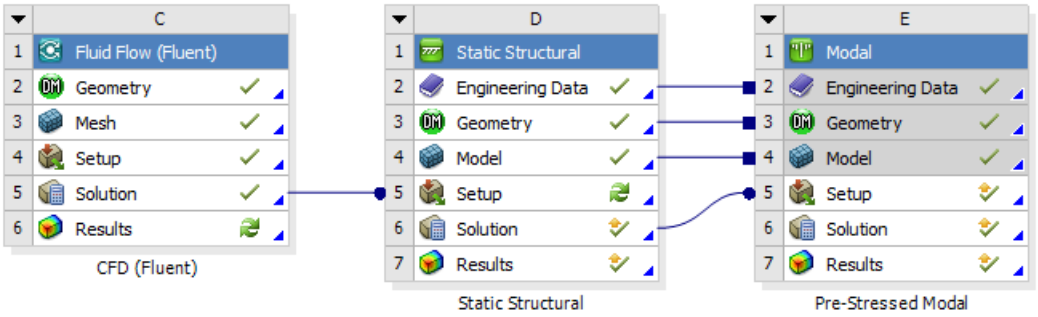

Figure 43: FEM analysis

CHAPTER 3

RESULTS

3.1 Effect of MFC patch on Static Analyses

As nature of MFC patch, when patch is loaded with a continuous input voltage load, patch deforms skin of blade statically. Therefore, as a checkpoint during constructing FE model, for a given input, it is expected to deform model angularly. Also, locations of MFC patches are determined in this step. Locations of MFC patches are determined with an iterative process and to obtain most effective locations on skin several analyses are performed. Determined locations of MFC patches are given at section xx and result of MFC patch at given locations with a 1500 V load in static analysis is given at Figure 44.

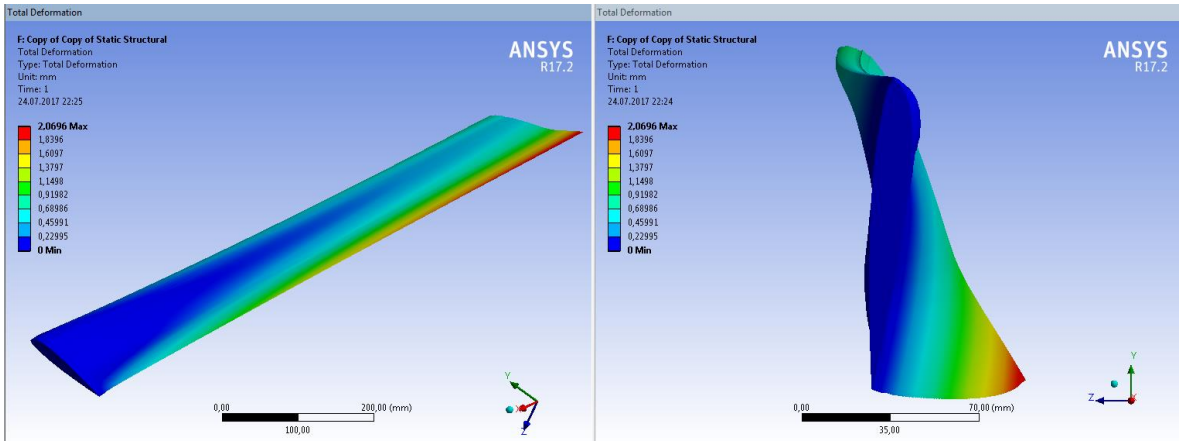

Figure 44: Total deformation of blade under 1500 V MFC load. (30x Magnified Results)

As it can be seen from figure, patch deforms blade angularly at static conditions, and effect of this patch on vibration is investigated at further sections.

3.2 Effect of MFC patch on Modal Analyses

Modal analyses are crucial part of this study. Evaluating modal analyses results, critical mode shape can be determined (1st Torsional Mode), critical frequency of 1st Torsional Mode can be determined, and also modal analyses gives an idea about how MFC Patch affects general dynamical behavior of helicopter blade.

Evaluating modal analyses results gives us 5th mode of blade is the 1st torsional mode which is target of this study. Modes of first 12 mode are given at table Table 5 and mode shape of fifth mode is given at Figure 45. Rest of mode shapes are given at Appendix A, also.

Table 5: Nominal values of blade natural frequency values

Mode Number	No MFC [Hz]
1	3,64
2	20,57
3	23,39
4	56,17
5	69,01
6	108,23
7	138,44
8	174,93
9	179,13
10	256,76
11	293,89
12	349,96

Note that during the performed analysis to get results at Table 5, MFC patch is added to model but no input is given. The main reason of adding the empty MFC patches to model is to consider change in mass after adding MFC to model. Therefore,

model at this state of analysis gives us to neglect change in mass for further results, and only effect of MFC inputs are investigated.

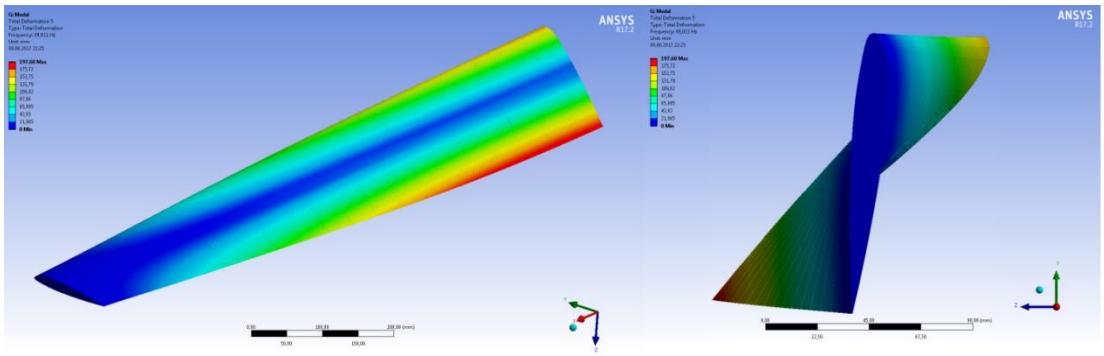

Figure 45: Mode shape of 5th mode of modal analysis (a.k.a. 1st Torsional Mode)

To investigate effects of MFC patch on resonant frequencies(daha iyi bir kelime bulunabilir) of blade several analyses are performed. During these analyses input of MFC patch is increased gradually and change in natural mode shape frequencies are investigated. Each analysis also used for further analyses as input of harmonic analyses and also gives an idea about determining study range of harmonic frequencies.

Effects of MFC Patch on modal frequencies for first 12 modes are given at table x12 and also visualized for first 6 modes on **Figure 46**.

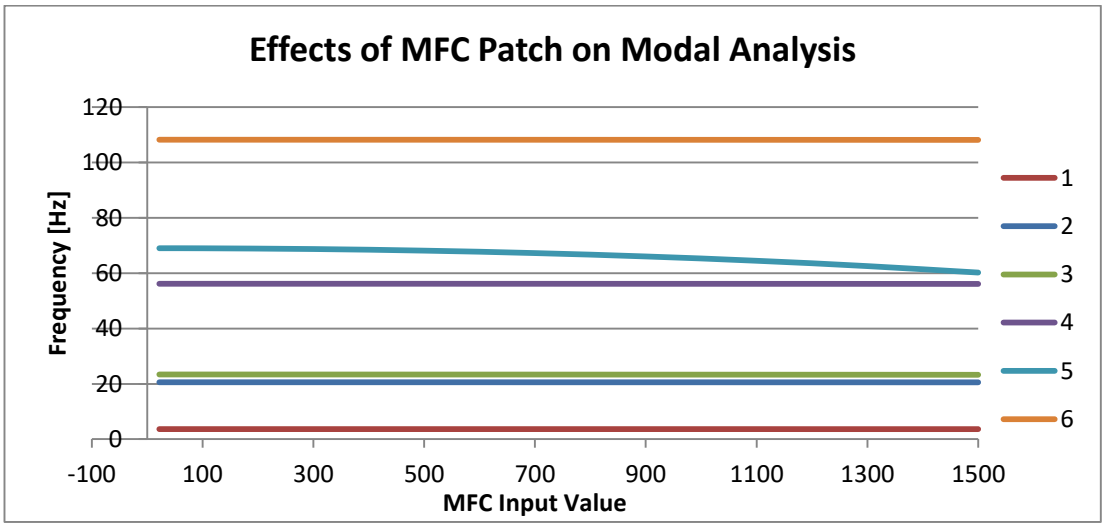

Figure 46: Effects of MFC patch on modal analysis

Table 6: Effects of MFC patch on modal frequencies

Mode Number	No MFC [Hz]	100 C [Hz]	300 C [Hz]	500 C [Hz]	700 C [Hz]	900 C [Hz]	1100 C [Hz]	1300 C [Hz]	1500 C [Hz]
1	3,64	3,64	3,64	3,64	3,64	3,64	3,64	3,64	3,63
2	20,57	20,57	20,57	20,57	20,57	20,56	20,56	20,55	20,54
3	23,39	23,39	23,38	23,37	23,36	23,34	23,32	23,30	23,27
4	56,17	56,17	56,17	56,16	56,16	56,15	56,14	56,13	56,11
5	69,01	68,99	68,72	68,14	67,25	66,04	64,48	62,55	60,22
6	108,23	108,23	108,22	108,22	108,21	108,20	108,19	108,18	108,16
7	138,44	138,43	138,41	138,38	138,34	138,31	138,27	138,22	138,17
8	174,93	174,92	174,89	174,84	174,75	174,61	174,40	174,10	173,65
9	179,13	179,12	179,03	178,85	178,58	178,24	177,85	177,44	177,05
10	256,76	256,76	256,74	256,73	256,71	256,69	256,67	256,64	256,62
11	293,89	293,88	293,80	293,66	293,45	293,16	292,81	292,39	291,89
12	349,96	349,95	349,93	349,91	349,88	349,86	349,83	349,80	349,77

Both from table and figure can be seen that MFC patch affects only 5th mode of blade which is a success for this study. Rest of modes has no change with given MFC input loads.

3.3 Effect on MFC Patch on Harmonic Analysis

Harmonic analyses are performed in two different aspects. Firstly, effects on various voltage inputs on patch are investigated. Performing this study helps us how patch affects and changes vibrations characteristics of blade at previous chapter. Now, with help of harmonic analyses, amplitudes on critical frequencies can also be investigated. For this part of study various application voltage inputs applied to FE model. Voltages are started from 100 V and increase with 200 V steps up to 1500 V which is MFC Patch's limit. Secondly, effect of patch's length is investigated. Patch is divided into 10 equal parts. During this part of study, effect of patch length is investigated. Study starts with %10 length of total patch and increased up to %100 of patch under 1500 V voltage input. Note that, at this part, patches are investigated

separately and while one patch is investigated, the other patch stays fully loaded with 1500 V input.

Results of effects various voltage inputs on MFC patch are given below. It is known that critical frequency of blade, which is 1st torsional mode, is 69.01 Hz. Therefore, at this part of study 69.01 Hz is evaluated. From Figure 47, it can be seen that behavior of blade on 69.01 Hz with given different voltage values. It is clearly seen that amplitude is decreased for given frequency. In addition, on top of that amount of decrease in amplitude at critical frequency can be seen from Figure 48.

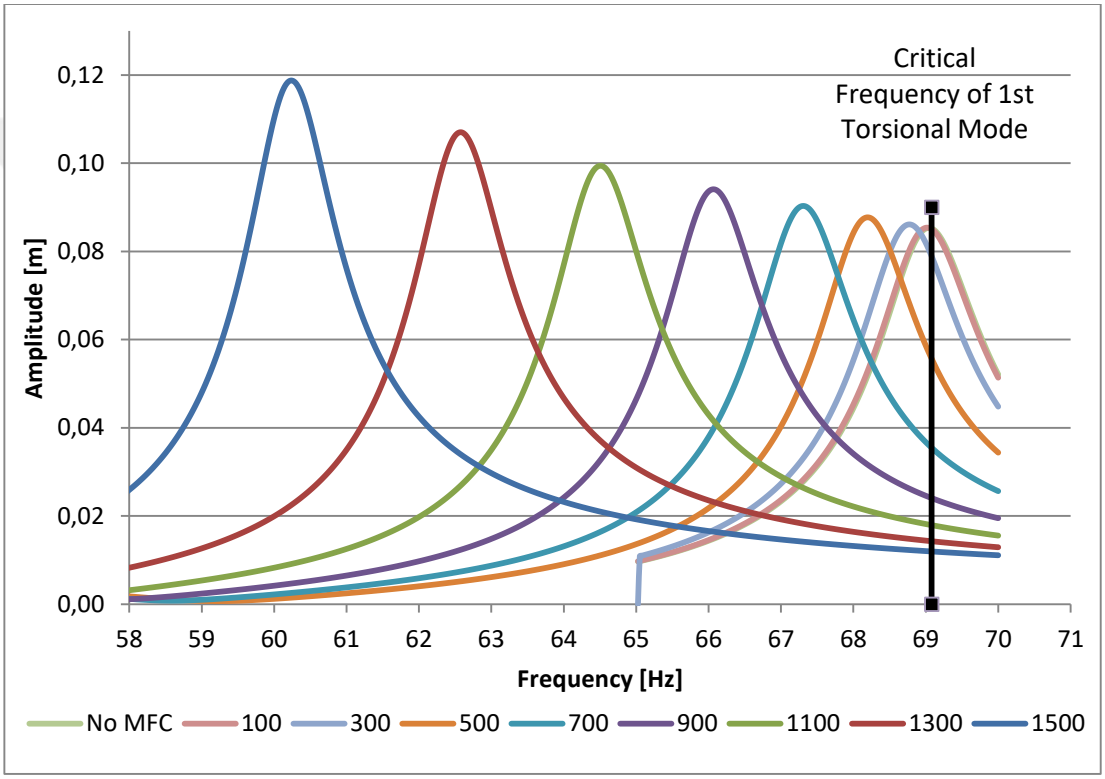

Figure 47: Amplitude vs Frequency figure for different voltage values on MFC application

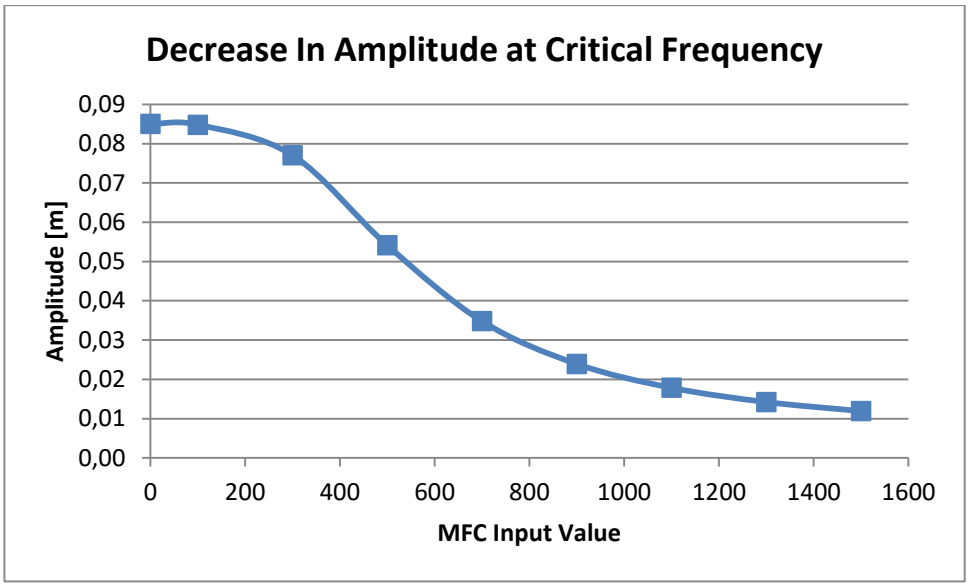

Figure 48: Amount of decrease in amplitude at 69.01 Hz

To investigate figures from numerical point of view, values of amplitudes at given voltage input values on MFC, amplitude values of blade at critical frequency of 1st torsional mode, 69.01 Hz, and decrease percentage of amplitude value relative to before applying MFC to model can be seen from Table 7 below.

Table 7: Decrease of amplitude under given various MFC input voltage load

Patch Input	Amplitude [m]	Decrease in %
No MFC	0,08504	0,0%
100	0,08481	0,3%
300	0,07705	9,4%
500	0,05412	36,4%
700	0,03481	59,1%
900	0,02393	71,9%
1100	0,01785	79,0%
1300	0,01423	83,3%
1500	0,01192	86,0%

Secondly, effectiveness of MFC is investigated on blade. To investigate this, patch model is divided into 10 equal parts as it can be seen at Figure 49 and Figure 50.

Both front and back side patch are investigated separately. Analyses started with only %10 of blade increased with %10 increments and effects on vibration reduction are investigated. Figure for front patch is can be seen below. Note that during these analyses, one MFC patch is divided and increased by %10, however, there is no changes applied to other MFC patch. Front and rear side of MFC patches are evaluated separately.

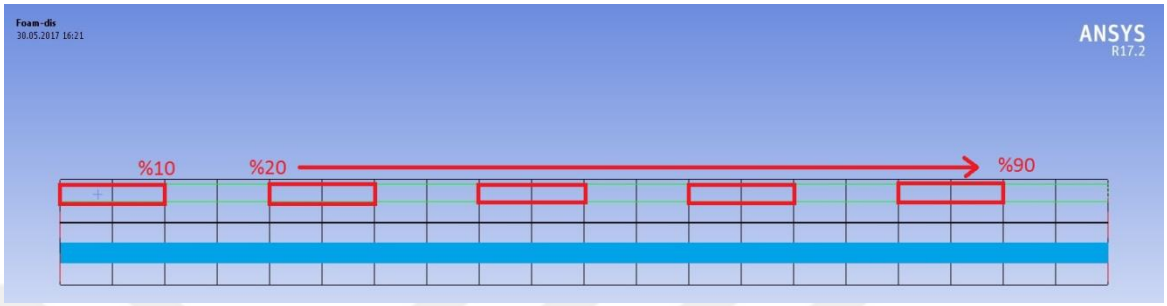

Figure 49: Patch division lengths and increment direction for front MFC Patch

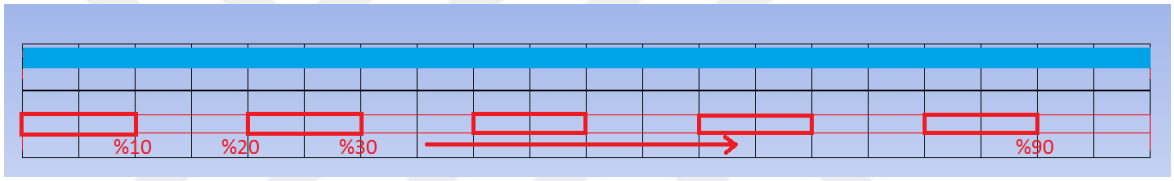

Figure 50: Patch division lengths and increment direction for rear MFC Patch

During comparison of values of amplitudes, each side evaluated with their own values which means MFC at %0 is no MFC patch input at given section but the other section of MFC patch is fully loaded with 1500 V. Afterwards, MFC patch is started to loaded incrementally in length during other side of MFC stays fully loaded at 1500V. Therefore, effect of MFC patch is evaluated separately for front and back and value of critical frequency at no MFC input will not be 69.01 Hz for given reason. According to Figure 51 and Figure 52, decrease of amplitude during MFC application can be seen.

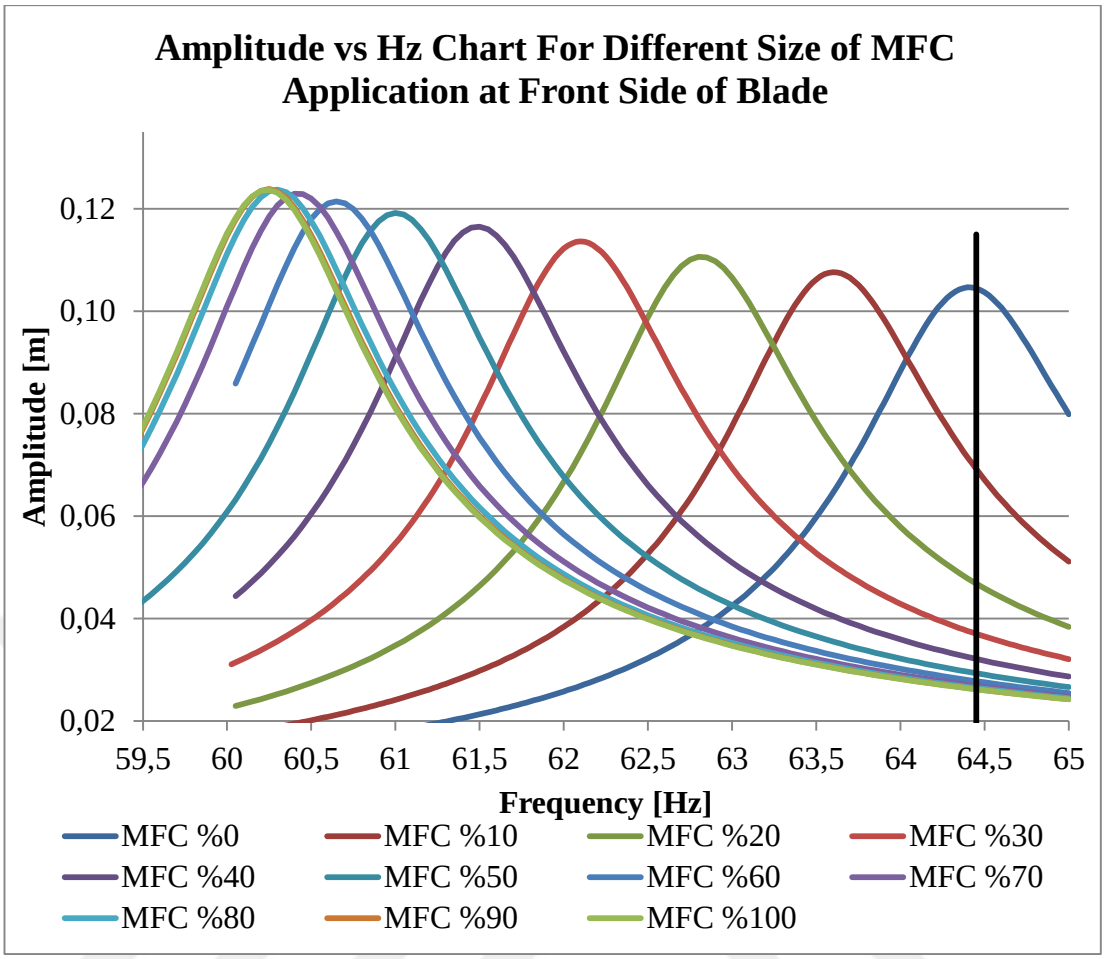

Figure 51: Decreases of amplitude for different amount of MFC application

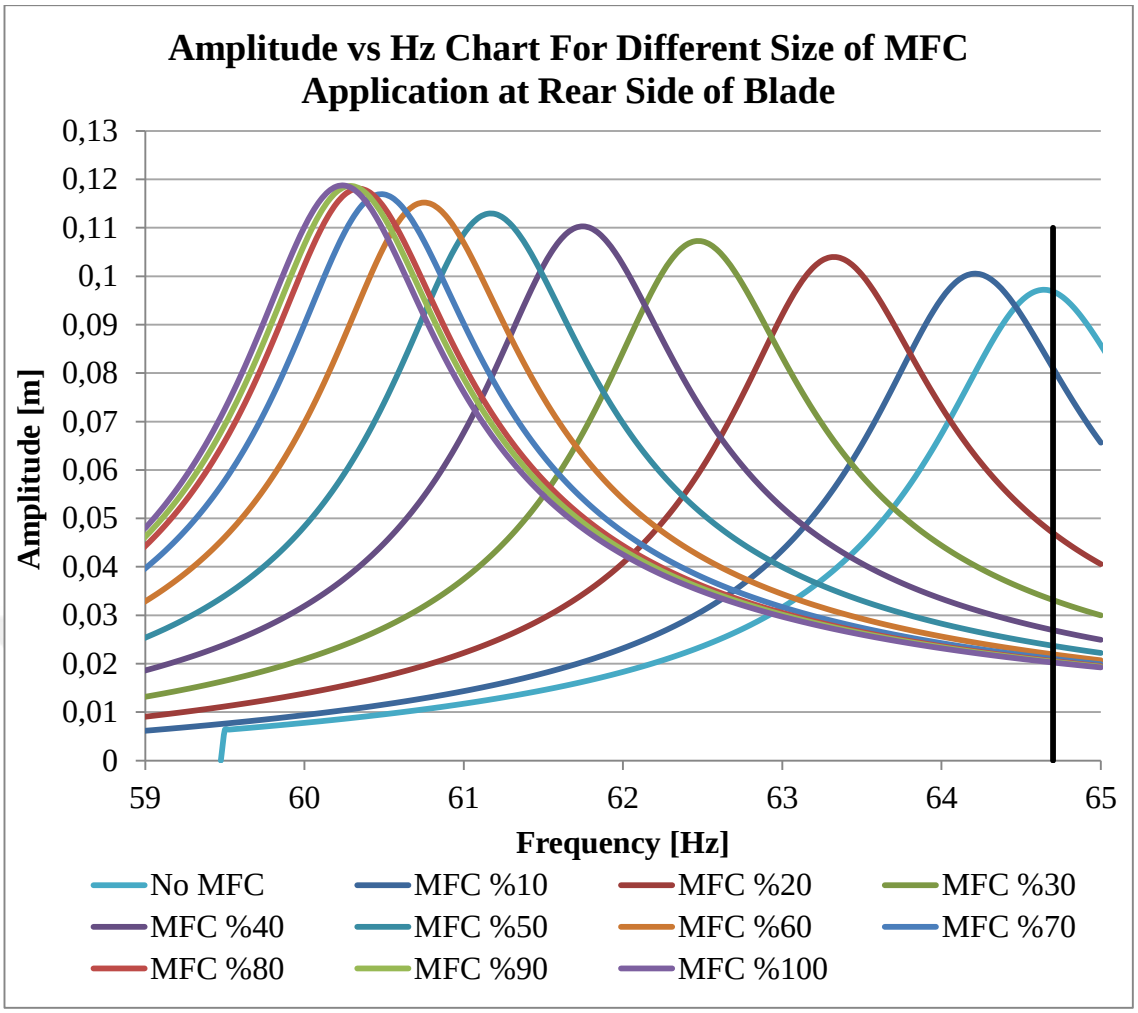

Figure 52: Amplitude vs Hz Chart For Different Size of MFC Application at Front Side of Blade

From both figures, it can be concluded that, when application length of MFC patch reaches to %70 of spar, effect of MFC patch is converges to a stable value and decrease in amplitude will not be affected too much. Therefore, it can be commented that if the purpose is only to decrease amplitude, application length of MFC patch is up to %70 percent may be enough. Generally, the amplitude will decrease by increasing amount of MFC application. Finally, results show that the length of piezoelectric actuators affects the active control of vibration.

3.3.1. Detailed Results for Effects of MFC Patch Length Analysis

3.3.1.1. Results of Front Side MFC Patch

In this chapter detailed results and plots of effects of MFC patch length on blade for static results are given. Plots are exaggerated with a scale factor of 10. Front and side view of results are given.

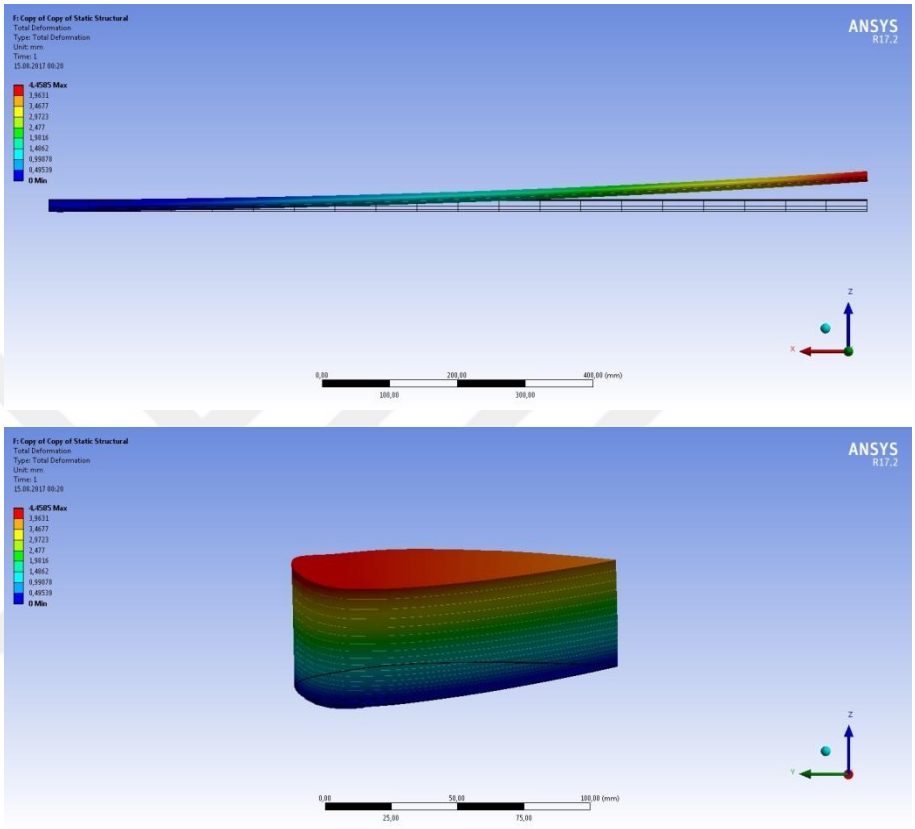

Figure 53: Static results of blade with no voltage input on front side of MFC

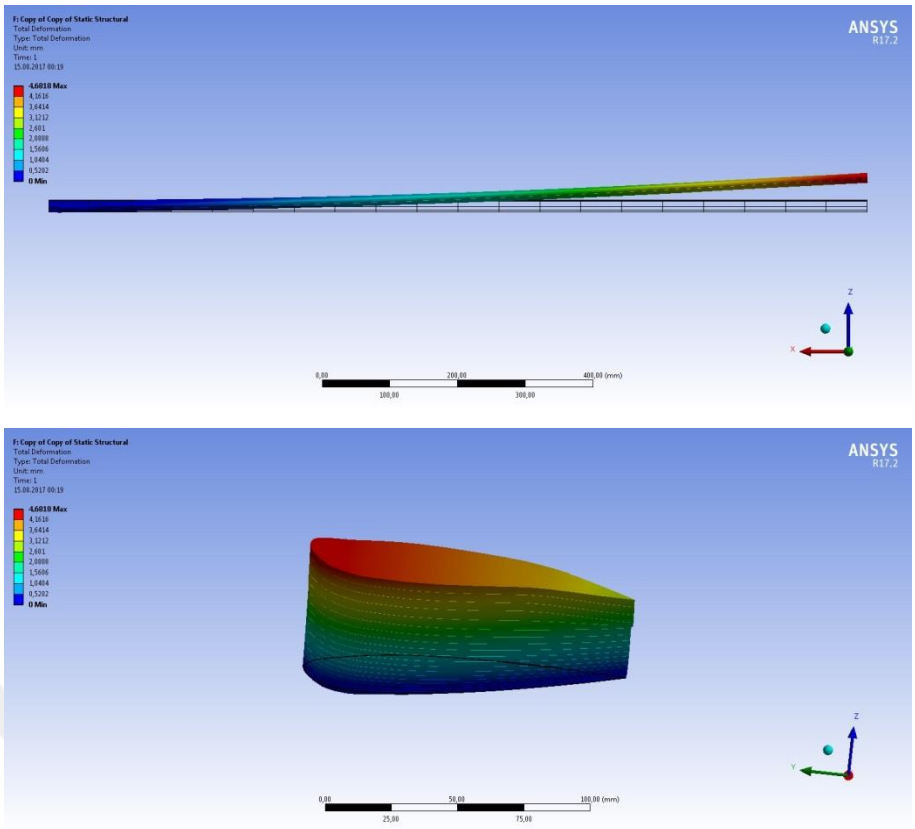

Figure 54: Static results of blade with %20 voltage input on front side of MFC

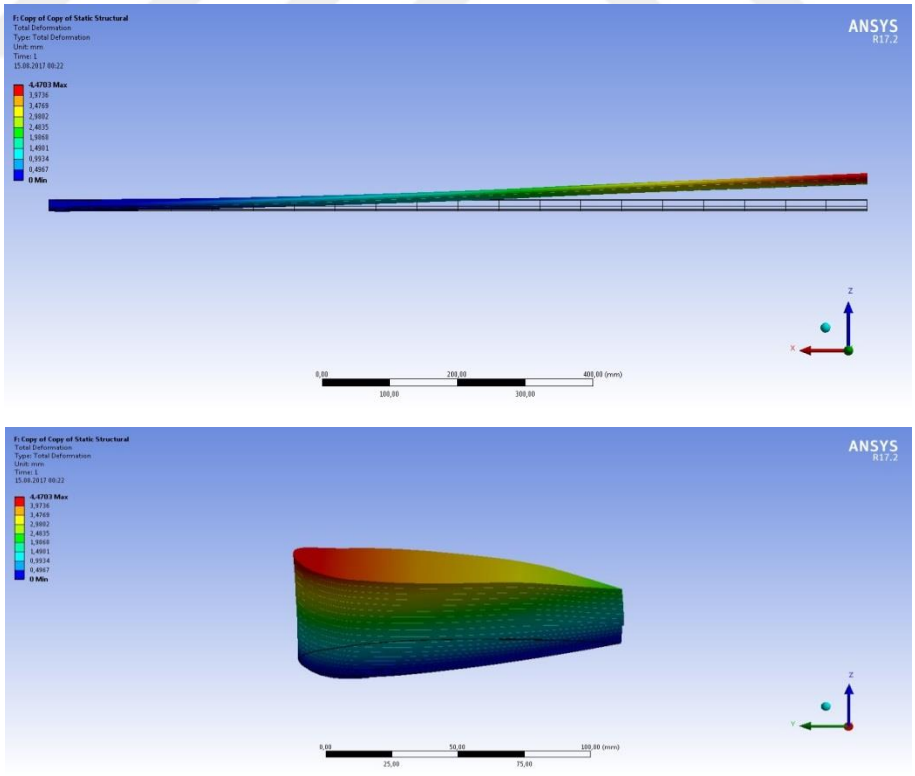

Figure 55: Static results of blade with %40 voltage input on front side of MFC

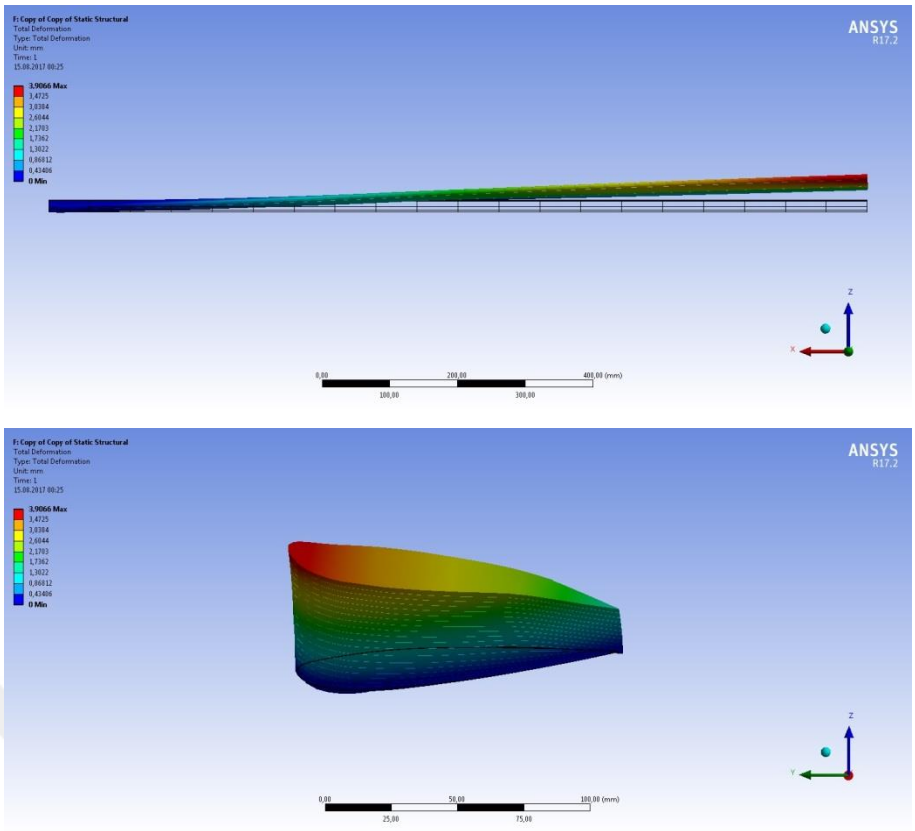

Figure 56: Static results of blade with %60 voltage input on front side of MFC

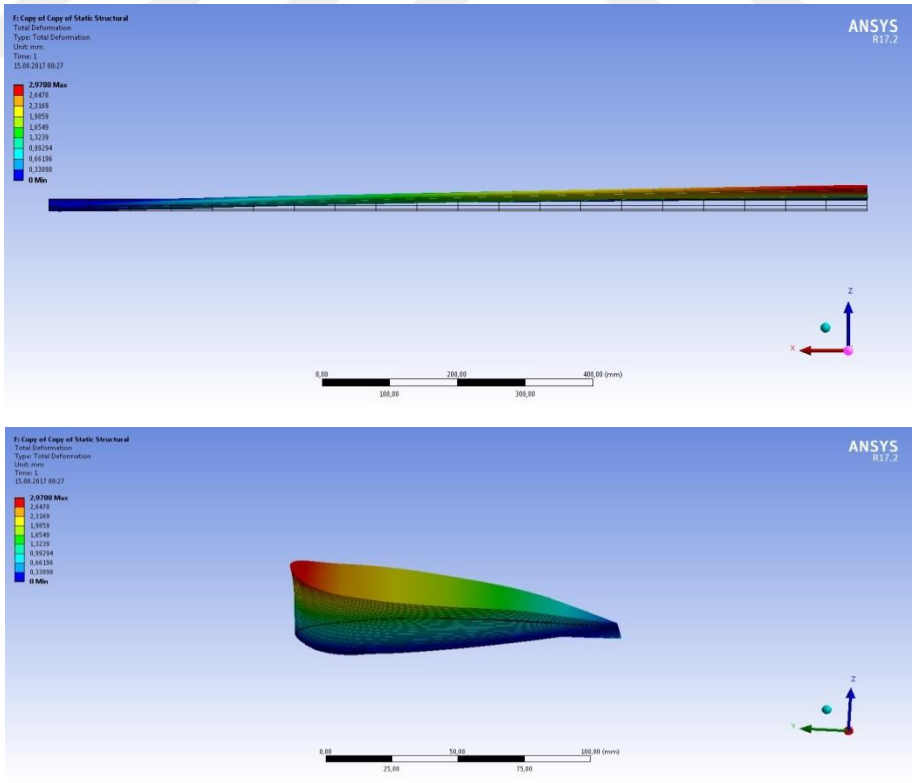

Figure 57: Static results of blade with %80 voltage input on front side of MFC